

1 **Continental pollution in the Western Mediterranean basin: vertical profiles of**  
2 **aerosol and trace gases measured over the sea during TRAQA 2012 and**  
3 **SAFMED 2013**

4 C. Di Biagio<sup>1</sup>, L. Doppler<sup>2,3,4</sup>, C. Gaimoz<sup>1</sup>, N. Grand<sup>1</sup>, G. Ancellet<sup>2</sup>, J.-C. Raut<sup>2</sup>, M. Beekmann<sup>1</sup>, A.  
5 Borbon<sup>1</sup>, K. Sartelet<sup>5</sup>, J.-L. Attié<sup>6,7</sup>, F. Ravetta<sup>2</sup>, and P. Formenti<sup>1</sup>

6 (\*corresponding author: claudia.dibiagio@lisa.u-pec.fr)

7  
8 <sup>1</sup> *LISA, UMR CNRS 7583, Université Paris Est Créteil et Université Paris Diderot, Institut Pierre*

9 *Simon Laplace, Créteil, France*

10 <sup>2</sup> *Sorbonne Universités, UPMC Univ. Paris 06; Université Versailles St-Quentin; CNRS/INSU,*

11 *LATMOS-IPSL, Paris, France*

12 <sup>3</sup> *Freie Universität Berlin, Berlin, Germany*

13 <sup>4</sup> *Deutscher Wetterdienst, Meteorological Observatory Lindenberg, Germany*

14 <sup>5</sup> *CEREA, Joint Laboratory École des Ponts ParisTech – EDF R & D, Université Paris-Est, 77455*

15 *Marne la Vallée, France*

16 <sup>6</sup> *Laboratoire d'Aérodologie, University of Toulouse, UMR 5560 CNRS, France*

17 <sup>7</sup> *CNRM GAME UMR 3589 CNRS, METEO-FRANCE*

18  
19 **Abstract**

20 In this study we present airborne observations of aerosol and trace gases obtained over the sea in the  
21 Western Mediterranean basin during the TRAQA (TRansport and Air QuAlity) and SAFMED  
22 (Secondary Aerosol Formation in the MEDiterranean) campaigns in summers 2012 and 2013. A  
23 total of 23 vertical profiles were measured up to 5000 m above sea level over an extended area

24 (40°-45°N latitude and 2°W-12°E longitude) including the Gulf of Genoa, Southern France, the  
25 Gulf of Lion, and the Spanish coast. During TRAQA and SAFMED the study area  
26 experienced successfully measured a wide range of meteorological conditions which  
27 favoured the pollution export from different sources located around the basin. Also, several events  
28 of dust outflows were measured during the campaigns. Observations from the present study  
29 indicateshow that continental pollution largely affects the Western Mediterranean both close to  
30 coastal regions and in the open sea as far as ~250 km from the coastline. ~~Aerosol layers not~~  
31 ~~specifically linked with Saharan dust outflows are distributed ubiquitously which indicates quite~~  
32 ~~elevated levels of background pollution throughout the Western basin.~~ The measured aerosol  
33 scattering coefficient varies between ~20 and 120 Mm<sup>-1</sup>, while carbon monoxide (CO) and ozone  
34 (O<sub>3</sub>) mixing ratios are in the range of 60-~~170~~-165 ppbv and 30-85 ppbv, respectively. Pollution  
35 reaches 3000-4000 m in altitude and presents a very complex and highly stratified structure  
36 characterized by fresh and aged layers both in the boundary layer and in the free troposphere.  
37 Within pollution plumes the measured particle concentration in the Aitken (0.004-0.1 μm) and  
38 accumulation (0.1-1.0 μm) modes is between ~100 and 5000-6000 scm<sup>-3</sup> (standard cm<sup>-3</sup>), which is  
39 comparable to the aerosol concentration measured in continental areas under pollution  
40 conditionseontinental urban areas. Additionally, our measurements indicate the presence of highly  
41 concentrated Aitken layers (10000-15000 scm<sup>-3</sup>) observed both close to the surface and in the free  
42 troposphere, possibly linked to the influence of new particle formation (NPF) episodes over the  
43 basin.

44

## 45 1. Introduction

46 Atmospheric aerosols play an important role on climate through their participation to several  
47 chemical, dynamical, and radiative processes. At present, still large uncertainties persist in the

48 estimation of the aerosol direct and indirect effects mainly due to the difficulty of fully  
49 characterizing their spatial and vertical distribution and properties (Boucher et al., 2013).

50 The Mediterranean region is a complex area where atmospheric aerosols of different origins and  
51 types may be found (Pace et al., 2006; Kallos et al., 2007; Gkikas et al., 2012). High levels of  
52 anthropogenic aerosol particles and pollutants are measured in the Mediterranean (Lelieveld et al.,  
53 2002), which is also indicated as one of the main hot spots for air quality issues (Monks et al.,  
54 2009).

55 The North-Western part of the Mediterranean basin, due to its proximity to highly polluted  
56 industrialized areas (such as the Po Valley in northern Italy and the Fos/Berre in southern France)  
57 and large coastal cities (Barcelona, Genoa, Marseilles, Nice, or Valencia), is frequently affected by  
58 continental outflows and severe pollution episodes (Mallet et al., 2005; Pérez et al., 2008; Pey et al.,  
59 2010). The strength of these episodes is particularly intense during summer when stable  
60 meteorological conditions and the high level of insolation promote photochemical reactions and the  
61 build-up of ozone and other pollutants (e.g. Millán et al., 2000).

62 A number of studies have investigated the dynamics of pollution export over the Western basin with  
63 the aim of characterizing the impact of anthropogenic emissions over this region. Most of these  
64 studies have been conducted in continental coastal areas and provide information on the vertical  
65 distribution of aerosols and their properties mainly close to local pollution sources. They include  
66 ground-based observations with lidars (Soriano et al., 2001; Pérez et al., 2004; Ancellet and  
67 Ravetta, 2005), and airborne campaigns, such as MECAPIP (MEso-meteorological Cycles of Air  
68 Pollution in the Iberian Peninsula) and RACAPMA (RegionAl Cycles of Air Pollution in the west  
69 central Mediterranean Area) in coastal Spain (Millán et al., 1996 and 1997) and ESCOMPTE  
70 (Experience sur Site pour Contraindre les Modeles de Pollution atmospherique et de Transport  
71 d'Emissions) in Southern France (Drobinski et al., 2007). The results of these studies have  
72 highlighted the important role of pollution in modulating the atmospheric composition in this part

73 of the basin, as well as the high variability of the aerosol distribution and properties in link to  
74 different export conditions (Flamant and Pelon, 1996; Soriano et al., 2001; Mallet et al., 2005). In  
75 particular, the interaction between synoptic circulation and local dynamics, such as orography and  
76 sea breezes, has been shown to strongly impact the vertical distribution, layering, and aging of  
77 particles along coastal regions (e.g. Millan et al., 1997; Gangoiti et al., 2001; Pérez et al., 2004;  
78 Velchev et al., 2011).

79 The capability of reproducing this complexity by air quality models represents a real challenge  
80 (Jimenez et al., 2006; Jiménez-Guerrero et al., 2008), and experimental observations gives a  
81 fundamental support to test the performances of the model outputs over the Western Mediterranean  
82 environment.

83 The large set of observations conducted in the last decades has permitted to acquire a detailed  
84 characterisation of pollution aerosols in the surroundings of the Western basin. However, at the  
85 present time we miss an extensive representation of the mean aerosol load, distribution, and  
86 properties in the whole region, in particular over the remote sea. In addition, there is a significant  
87 lack of observations over some key areas, as for example the Gulf of Genoa, directly under the  
88 influence of the outflow from the highly polluted Po Valley (Velchev et al., 2011).

89 In this study we present measurements of aerosols and trace gas vertical profiles acquired during 24  
90 scientific flights performed with the ATR-42 French research aircraft during the TRAQA  
91 (TRansport and Air QuAlity) and SAFMED (Secondary Aerosol Formation in the MEDiterranean)  
92 campaigns in summers 2012 and 2013 in the framework of the Chemistry-Aerosol Mediterranean  
93 Experiment (CHARMEX, <https://charmex.lsce.ipsl.fr/>). The TRAQA and SAFMED flights  
94 explored an extended region of the Western Mediterranean basin between 40°-45°N latitude and  
95 2°W-12°E longitude including the Gulf of Genoa, Southern France, the Gulf of Lion, and the  
96 Spanish coasts. Measurements were performed over the sea at various distances from the coastline  
97 with lidar and in situ instruments. During TRAQA and SAFMED the Western basin was **interested**

98 | ~~by~~under diverse synoptic conditions which led to the occurrence of different pollution export  
99 regimes (Mistral/Tramontane events, outflow from the Po Valley and the Iberian Peninsula) and  
100 allowed sampling atmospheric aerosols of different origin and types.

101 | The main objective of the present work is to provide ~~extensive~~ observations of the vertical  
102 distribution of aerosols and trace gases related to the export of anthropogenic pollution at the  
103 regional scale of the Western Mediterranean basin. The detailed knowledge of the vertical structure  
104 of the atmosphere is very important to understand the impact of continental pollution over the basin.  
105 The paper is organized as follows: in Sections 2, 3, and 4 we describe the flight trajectories and  
106 strategy during TRAQA and SAFMED, the in situ measurements carried out on board the ATR-42  
107 aircraft, and the meteorological conditions observed during the campaigns. In Sect. 5 we present the  
108 results. The aerosols and trace gases vertical profiles are shown in Sections 5.1 and 5.2. Section 5.3  
109 is dedicated to analyse the variability of the pollution plume composition and atmospheric structure  
110 also in link with the different outflow conditions. Airborne measurements in presence of layers with  
111 high concentrations of fine particles are discussed in Section 5.4. The main conclusions are reported  
112 in Section 6.

113

## 114 2. Overview over flights

115 Figure 1 shows the trajectories of the flights performed during the TRAQA (20 June-13 July 2012)  
116 and the SAFMED (24 July-1 August 2013) campaigns. Research flights were performed with the  
117 SAFIRE (Service des Avions Français Instruments pour la Recherche en Environnement,  
118 <http://www.safire.fr/>) tropospheric aircraft ATR-42. The aircraft has a maximum endurance of 4 h.  
119 The flight altitude ranges between a minimum of ~60 m over the sea, to a maximum of ~5000 m  
120 above sea level (a.s.l.). The aircraft was based in Toulouse (43°36'N, 1°26'E, France) during  
121 TRAQA and in Genoa (44°24'N, 8°55'E, Italy) during SAFMED. Twenty-four flights for a total of  
122 ~75 hours of data have been collected. Seventeen of the twenty-four flights presented in the paper

123 were performed during TRAQA (flight numbers V16 to V32) and 7 during SAFMED (V46 to  
124 V52). All flights were carried out during daytime, when light-induced chemistry favours the  
125 pollution levels. Frequently, two flights per day, with intermediate stops in different airports in  
126 Southern France, Corsica, and Sardinia, were performed. The majority of flights were over the sea,  
127 with some exceptions investigating inland areas in Southern France and central Italy. Main  
128 information concerning the TRAQA and SAFMED flights is summarized in Table 1.

129 The general flight strategy consisted in plane flights with lidar observations and vertical  
130 ascents/descents to sound the vertical atmospheric column (from ~60-100 m to 3000-5000 m a.s.l.)  
131 and identify main meteorological and aerosol features, followed by straight levelled runs (SLRs)  
132 within the detected aerosol layers. In this study we focus on vertical profiles data. A total of 23  
133 profiles were acquired in 20-30 minutes each by performing a spiral trajectory ~10-20 km wide.  
134 Fig. 1 also identifies the geographical position of each sounding. As shown in Fig. 1 the profiles  
135 were performed at different distances from the coastline, from a minimum of ~5-10 km for V31 and  
136 V32 to more than ~250 km for V20 and V25, and covered almost all the different sectors of the  
137 Western basin.

138

### 139 **3. Measurements and methods**

140 The basic equipment of the ATR-42 aircraft includes sensors for the measurements of  
141 meteorological parameters (pressure, temperature, relative humidity, wind components), radiative  
142 fluxes (down- and up-welling shortwave and longwave radiation), and carbon monoxide (CO) and  
143 ozone (O<sub>3</sub>) mixing ratios.

144 Aerosol sampling was performed using the AVIRAD system (Formenti et al., 2011). AVIRAD is an  
145 iso-axial and iso-kinetic inlet which, at the normal cruise speed of the ATR-42 (~93 m s<sup>-1</sup>), samples  
146 air at a volumetric flow of ~350 l min<sup>-1</sup>. The 50% passing efficiency of the inlet was tested to be 12  
147 μm diameter. Various sampling lines depart from AVIRAD to connect to different instruments

148 mounted inside the aircraft cabin: (i) a 3-wavelength nephelometer (TSI Inc., model 3563) for the  
149 measurement of the dry particle volume total scattering ( $\sigma_s$ ) and hemispherical backscattering ( $\sigma_{bs}$ )  
150 coefficients at 450, 550, and 700 nm; (ii) a 7-wavelengths aethalometer (Magee Sci., model AE31)  
151 for the measurement of the particle absorption coefficient ( $\sigma_a$ ) at 370, 470, 520, 590, 660, 880, and  
152 950 nm; (iii) an optical particle counter ~~(OPC)~~ (GRIMM Inc., model 1.129) for the measurement of  
153 the particle number concentration over 32 size classes between 0.3 and 32  $\mu\text{m}$  in diameter; (iv) a  
154 Condensation Particle Counter (CPC, TSI Inc., model 3775) for the measurement of the total  
155 particle number concentration in the diameter range 0.004-3.0  $\mu\text{m}$ ; and (v) 3 lines for aerosol  
156 sampling on filter membranes and a 4-stage cascade impactor (Dekati Inc) to measure the bulk and  
157 size-segregated particle composition. In addition, the ATR-42 was equipped with a Passive Cavity  
158 Aerosol Spectrometer Probe (PCASP, model 100X) ~~OPC~~ optical particle counter for the  
159 measurement of the aerosol number concentration over 31 size classes between 0.1–3.0  $\mu\text{m}$ . The  
160 PCASP was installed outside the cabin on the left side of the aircraft fuselage.

161 In this study we consider measurements of the (i) aerosol scattering coefficient from the  
162 nephelometer, (ii) particle concentration from the CPC and PCASP instruments (GRIMM data are  
163 not considered since they are available only below ~350 m during TRAQA), (iii) CO and O<sub>3</sub> trace  
164 gases from the MOZART analyser, and (iv) meteorological parameters from the ATR-42 sensors. A  
165 more detailed description of the nephelometer, CPC, PCASP, and MOZART measurements and  
166 their data analysis is provided in the following sections.

167 The present analysis is based only on measurements obtained in cloud free conditions.

168

### 169 **3.1 Aerosol scattering coefficient**

170 A three-wavelength integrating nephelometer has been used to measure the dry particle volume  
171 total scattering ( $\sigma_s$ ) coefficient at 450, 550, and 700 nm. The sampling flow rate was 30 l min<sup>-1</sup>.  
172 Data were acquired at 6 s resolution during TRAQA and 1 s resolution during SAFMED. The

173 instrument was calibrated prior ~~the~~each campaign with free-particle air and CO<sub>2</sub> as gases of low  
174 and high known scattering coefficient. Nephelometer measurements have been corrected for angular  
175 truncation and Lambertian non-idealities by applying the formulae by Anderson and Ogren (1998).  
176 The measurement uncertainty on  $\sigma_s$  is calculated taking into account for the photon counting, gas  
177 calibration, and angular corrections uncertainties (Anderson et al., 1996; Anderson and Ogren,  
178 1998). The total uncertainty on  $\sigma_s$  is estimated to be lower than 10% at the three wavelengths.

179 The nephelometer measured the scattering coefficient in dry air conditions. This is due to the  
180 heating of the airflow while entering the aircraft cabin and the temperature in the cavity of the  
181 instrument. The relative humidity measured during the flights inside the nephelometer was <25% in  
182 more than ninety percent of cases, with values up to ~40% occasionally observed at very low  
183 altitudes (<200 m) over the sea surface. A possible underestimation of the scattering coefficient  
184 may thus occur in case of hygroscopic aerosols, especially under high relative humidity conditions  
185 in the atmosphere.

186 The particle scattering Ångström exponent ( $\alpha_s$ ) has been calculated from spectral nephelometer  
187 measurements with a power-law fit of the measured scattering coefficients versus wavelength.

188

### 189 **3.2 Aerosol particle number concentration**

190 The vertical profiles of the total particle number concentration in the Aitken ( $dN_{\text{Aitken}}$ , 0.004-~~nm~~0.1  
191  $\mu\text{m}$ ), accumulation ( $dN_{\text{Acc}}$ , 0.1-1.0  $\mu\text{m}$ ) and coarse ( $dN_{\text{Coarse}}$ , >1.0  $\mu\text{m}$ ) modes have been obtained  
192 by combining CPC and PCASP data. The CPC and the PCASP measured at a sample flow of 1.5  
193 and 0.06 l min<sup>-1</sup>, respectively, and with a time resolution of 1 s for the PCASP and 5 s and 1 s for  
194 the CPC during TRAQA and SAFMED, respectively.

195 The PCASP was factory calibrated with monodisperse polystyrene sphere latex (PSL) whose  
196 complex refractive index at the instrument operating wavelengths (632.8 nm) is 1.59-0i. The



197 measured sphere-equivalent optical diameter has been converted to a sphere-equivalent geometrical  
198 diameter ( $D_g$ ) by taking into account the complex refractive index of the sampled aerosol (Liu and  
199 Daum, 2000). Given that in the very large majority of cases the aerosol sampling during TRAQA  
200 and SAFMED was associated to the export of pollution plumes, only pollution aerosols have been  
201 considered for ~~OPC~~PCASP correction. Note that these data are not optimized for dust or marine  
202 aerosol observations. A large interval of values ( $n \sim 1.50-1.72$ ,  $k \sim 0.001-0.1$  for UV-visible  
203 wavelengths) are reported in the literature for the real and the imaginary parts of the refractive index  
204 for anthropogenic aerosols over Europe (e.g., Ebert et al., 2002 and 2004; Müller et al., 2002;  
205 Mallet et al., 2003 and 2011; Chazette et al., 2005; Raut and Chazette, 2008). For our calculations at  
206 632.8 nm we have fixed the imaginary part of the refractive index to 0.01, thus representing a mean  
207 absorbing aerosol, and then we have varied the real part between its minimum (1.50) and maximum  
208 (1.72) reported value.  $D_g$  is then set at the mean  $\pm$  one standard deviation of the values obtained for  
209 the different values of  $n$ . We assume in these calculations that the refractive index does not vary  
210 with height. After refractive index correction the  $D_g$  range for the PCASP becomes 0.10-4.47  $\mu\text{m}$ ,  
211 with an uncertainty between 1 and 25%. The smallest and the largest size bins of the ~~OPC~~PCASP,  
212 for which the minimum and maximum edges respectively are not defined, have been excluded from  
213 the datasets, thus reducing the PCASP  $D_g$  range to 0.11-4.17  $\mu\text{m}$ .

214 Once corrected for the refractive index, PCASP data have been combined with those from the CPC  
215 to calculate  $dN_{\text{Aitken}}$ ,  $dN_{\text{Acc}}$ , and  $dN_{\text{Coarse}}$ . Values for  $dN_{\text{Acc}}$  and  $dN_{\text{Coarse}}$  are obtained by integrating  
216 the PCASP number concentrations in the 0.1-1.0  $\mu\text{m}$  and 1.0-4.17  $\mu\text{m}$  ranges, while  $dN_{\text{Aitken}}$  is  
217 estimated as the difference between CPC concentration and the integral of PCASP data between 0.1  
218 and 3.0  $\mu\text{m}$ . The comparison between the PCASP and the GRIMM below 350 m altitude indicates  
219 that the former underestimates by about 50% the aerosol concentration in the range 0.4-1.0  $\mu\text{m}$  (the  
220 accuracy of the GRIMM has been verified by optical closure study against simultaneous aircraft  
221 nephelometer measurements). This is estimated to induce a  $\sim 20\%$  underestimation of the  $dN_{\text{Acc}}$

222 calculated here. Conversely, the PCASP underestimation in the 0.4-1.0  $\mu\text{m}$  range has almost a  
223 negligible impact on  $\text{dN}_{\text{Aitken}}$ .

224 CPC measurements, and so  $\text{dN}_{\text{Aitken}}$  data, were not available during SAFMED flights V49, V50, and  
225 part of V51.

226

### 227 **3.3 Trace gases**

228 Carbon monoxide (CO) and ozone ( $\text{O}_3$ ) mixing ratios were measured by the MOZART instrument  
229 described in detail by Nedélec et al. (2003). CO is a long-lived tracer for air masses influenced by  
230 combustion processes, whereas  $\text{O}_3$  in the troposphere is a photochemical product of the oxidation of  
231 CO and volatile organic compounds (VOCs) in the presence of nitrogen oxides ( $\text{NO}_x$ ). CO and  $\text{O}_3$   
232 are measured at a resolution of 30 s and 4 s, respectively. The nominal uncertainty is  $\pm 5\%$  for CO  
233 and  $\pm 2\%$  for  $\text{O}_3$  (Nedélec et al., 2003). However, a recent airborne intercomparison in May 2014 in  
234 the framework of the French ChemCalInt project and the TGOE European Joint Research Activity  
235 has suggested a greater uncertainty (up to 30%) on CO measurement by MOZART on-board the  
236 ATR-42 (A. Borbon, personal communication, 2015). Trace gas analysis will focus mostly on the  
237 vertical distribution of the  $\Delta\text{O}_3/\Delta\text{CO}$  ratio rather than absolute concentrations (see section 5.3) and  
238 the uncertainty on CO should not affect data interpretation.

239

### 240 **3.4 STP conversion**

241 In order to compare measurements obtained at different altitudes the data presented here are  
242 reported at standard temperature and pressure (STP) using  $T=293.15\text{ K}$  and  $p=1013.25\text{ hPa}$  (NIST,  
243 National Institute of Standards and Technology, values). Hence, the scattering coefficient is scaled  
244 to STP conditions and the particle concentrations are given as particles per standard  $\text{cm}^{-3}$  ( $\text{scm}^{-3}$ ).

245 For a generic parameter  $x$  measured at the temperature  $T$  and pressure  $p$ , the conversion at STP is  
246 ~~done-calculated~~ with the formula:

$$247 \quad x(\text{STP}) = x(T, p) \frac{T}{293.15} \frac{1013.25}{p} \quad (1).$$

248 CO and O<sub>3</sub> do not need to be corrected for STP since the mixing ratio does not depend on  
249 temperature and pressure.

250

### 251 3.5 Meteorological parameters

252 The vertical profiles of the pressure ( $p$ ), the temperature ( $T$ ), the relative humidity (RH) and the  
253 wind components towards the east and the north ( $U$ ,  $V$ ) measured on board the ATR-42 have been  
254 used to analyse the atmospheric structure during flights. Starting from the measured parameters the  
255 potential temperature ( $\theta$ ) has been also calculated as  $\theta = T(p_0/p)^{0.286}$  with  $p_0=1013.2$  mbar. For  
256 each profile the height of the marine aerosol boundary layer (MABL) and planetary boundary layer  
257 (BL) has been estimated visually by looking at the vertical gradients of  $T$ ,  $\theta$ , and RH.  
258 Meteorological parameters have been also used to calculate the vertical profiles of the gradient  
259 Richardson number (Ri):

$$260 \quad \text{Ri} = \frac{g}{\theta} \frac{\partial \theta}{\partial z} \bigg/ \left( \left( \frac{\partial U}{\partial z} \right)^2 + \left( \frac{\partial V}{\partial z} \right)^2 \right) \quad (2).$$

261 In Eq. (2)  $g$  is the gravitational acceleration and  $z$  is the height. The Ri number is the ratio between  
262 the buoyancy force and the wind shear and it is used to indicate dynamic stability and the formation  
263 of clear air turbulence. Turbulence can develop when Ri is below the critical threshold  $\text{Ri}_{\text{crit}}=0.25$ ,  
264 while it is inhibited for  $\text{Ri}>1$  (e.g., Wallace and Hobbs, 2006). In this study the profiles of Ri are

265 used to provide indications of favorable/unfavorable conditions for the development of turbulent  
266 conditions within the atmosphere.

267

### 268 **3.6 Tracking the air mass back-trajectories**

269 The Lagrangian trajectory model FLEXTRA (FLEXible TRAjectories, Stohl et al., 1995) has been  
270 used in selected cases to track the origin of sampled air masses. Five days three-dimensional back-  
271 trajectories have been calculated using the ECMWF (European Centre for Medium-Range Weather  
272 Forecast) operational analysis with a  $0.5^\circ$  by  $0.5^\circ$  horizontal resolution and up to 30 vertical model  
273 levels below 4000 m. The model specific humidity and potential vorticity is also interpolated along  
274 the trajectory path.

275

## 276 **4. Meteorological conditions, aerosol load, and pollution export regimes**

277 In order to characterize the general aerosol conditions encountered over the Western Mediterranean  
278 basin during the TRAQA and the SAFMED campaigns we have plotted the time-series of the  
279 aerosol optical depth ( $\tau_{\pm 0.02}$ ) at 440 nm and the 440-870 nm Ångström exponent ( $\alpha$ ) measured  
280 with a Cimel sunphotometer (Holben et al., 1998) at the three AERONET stations of Barcelona,  
281 Frioul, and Ersa located along the coast around the Western basin (see Fig. 1). Level 1.5 cloud-  
282 screened data are used in this study. Data are shown in Fig. 2 and correspond to the period of the  
283 campaign of measurements plus 10 days before and after. Table 1 reports the date, location, and  
284 main meteorological and export conditions encountered during TRAQA and SAFMED flights.

285

286 ~~The TRAQA campaign in 2012 was characterized by very variable meteorological conditions which~~  
287 ~~prevented the accumulation of high levels of pollutants over the basin. Over the analysed~~  
288 AERONET sites ~~t~~The aerosol optical depth was below 0.2 before the beginning of the TRAQA

289 campaign ~~over the whole basin~~ and increased, especially at Barcelona and Ersar, to ~0.3-0.5 (with  
290  $1 < \alpha < 2$ ) in the periods 23-26 June and 3-13 July 2012. Isolated peaks of  $\tau$  were measured in  
291 correspondence of two Saharan dust intrusion events which occurred on the 17-23 June ( $\tau \sim 0.6$ ) and  
292 29 June 2012 ( $\tau \sim 1.4$ ). Different wind regimes occurred during TRAQA and favoured the  
293 continental outflow from different regions located around the basin. Two examples of wind maps  
294 derived from WRF-Chem model (Grell et al., 2005) at 925 mbar are shown in Fig. 3 for 26 June and  
295 3 July 2012. Main observed meteorological/export conditions can be summarized as follows: (i) on  
296 26-27 June north/north-~~w~~easterly winds blew across northern Italy determining an air mass outflow  
297 towards the Gulf of Genoa (measurements on flights V18-V19-V21); (ii) on the same days a strong  
298 Mistral-Tramontane episode (i.e., strong northerly winds developing along the Rhône and Aude  
299 valley which bring a northerly/north-westerly flow over the Western Mediterranean, see Fig 3a)  
300 favoured the dispersion of pollutants towards the central part of the Western basin. Measurements  
301 during the event were performed during flight V20; (iii) on 3-4 July the wind regime was dominated  
302 by westerly/south-westerly winds mostly blowing at the surface across the Iberian Peninsula and  
303 southwestern France (see Fig. 3b). This condition allowed measuring the export of pollution from  
304 the Spanish coasts, in particular close to the area of Barcelona (flights V24-V25-V26, see Fig. 31).  
305 Additionally, flight V31 sounded the atmospheric structure close to the Spanish coasts -reaching the  
306 southern urban area of Valencia. The flight was performed under the influence of south-westerly  
307 winds favouring the export from the Iberian Peninsula towards the basin; (iv) ~~moderate~~-Mistral  
308 episodes occurred on the 6-7 and 11 July 2012. In those cases the Mistral wind combined with a  
309 persistent westerly flow thus yielding pollution export towards the central and central-eastern part  
310 of the Western basin, as measured during flights V27-V28-V30-V32; (v) finally, Saharan dust  
311 aerosols were sampled during flights V16 and V20 (episode of the 17-23 June) and flights V22 and  
312 V23 (episode of the 29 June).

313 During SAFMED the meteorological conditions were more stable and two distinct phases were  
314 observed: (i) a stable anticyclone affected the whole Western Mediterranean area during the first  
315 half of July until the 26th, thus possibly favouring a more pronounced accumulation of  
316 photochemical pollution in this part of the basin. Relatively high values of both  $\tau$  (~0.2-0.8) and  $\alpha$   
317 (~1-2.5) were measured at the three sites of Barcelona, Frioul, and Ersa in this period; (ii) a  
318 cyclonic system moving from the Atlantic region towards Europe then affected the Western basin  
319 on 28-29 July 2013. Very clean conditions ( $\tau < 0.1-0.2$ ) were measured afterwards over the entire  
320 region until the end of the SAFMED campaign. Winds were mostly westerly/south-westerly in the  
321 first period of the campaign (24-29 July 2013, flights V46, V47, V48, V49, V50), which means that  
322 the sampled air flow came mostly from the sea. Then, from 30 July to 1 August 2013 a north-  
323 easterly flow affected the SAFMED investigated area thus promoting the export of pollution from  
324 Northern Italy towards the Gulf of Genoa (flights V51, V52). A strong Mistral event (29 July-1  
325 August) and two Saharan dust outbreaks (27-28 July and 1 August) affected the Western basin,  
326 however not influencing the vertical profile observations during SAFMED.

327 In order to identify the distribution of observations during TRAQA and SAFMED as a function of  
328 the aerosol type we have plotted in Figure 4 the distribution of the measured scattering coefficient  
329  $\sigma_s$  at 450, 550, and 700 nm as a function of the calculated scattering Ångström exponent  $\alpha_s$  for all  
330 vertical profiles. The plot shows a similar scattering intensity between cases dominated by coarse  
331 particles ( $\alpha_s < 0.5-1.0$ ), such as desert dust, and those dominated by fine particles ( $\alpha_s > 1.0-1.5$ ), such  
332 as pollution aerosols. For both dust and pollution  $\sigma_s$  peaks at about 100-120  $\text{Mm}^{-1}$ . The frequency of  
333 occurrence of  $\alpha_s$  shows that pollution plumes represent the large majority of the cases observed,  
334 with more than 70% of measurements with  $\alpha_s > 1.0$ .

335

## 336 5. Results

337 Figure 5 shows the box and whisker plots of the aerosol scattering coefficient  $\sigma_s$  at 450, 550, and  
338 700 nm, particle number concentration in the Aitken ( $dN_{\text{Aitken}}$ ) and accumulation ( $dN_{\text{Acc}}$ ) and coarse  
339 ( $dN_{\text{Coarse}}$ )-diameter ranges, and CO and O<sub>3</sub> measured in the boundary layer (BL) and in the free  
340 troposphere (FT) within pollution plumes for all the different vertical soundings analysed in this  
341 study. This plot summarizes the range of values observed during TRAQA and SAFMED. On  
342 average, the scattering coefficient and CO are larger in the BL compared to the FT, whilst similar  
343 ranges of values are measured in the two regions for  $dN_{\text{Aitken}}$ ,  $dN_{\text{Acc}}$ , and O<sub>3</sub>. Even within the single  
344 BL and FT the different parameters show a large variability that will be explored in the following  
345 paragraphs.

346

### 347 **5.1 Vertical profiles of aerosol concentration and scattering coefficient**

348 Figure 6 shows the vertical profiles of  $\sigma_s$ ,  $dN_{\text{Acc}}$ , and  $dN_{\text{Coarse}}$  during TRAQA and SAFMED flights.  
349 The date, time and coordinates of each profile, as well as the heights of the top of the marine and  
350 planetary boundary layer (MABL and BL) estimated from meteorological data are also indicated in  
351 the plot.

352

353 For the different vertical soundings the particle concentrations  $dN_{\text{Acc}}$  and  $dN_{\text{Coarse}}$  vary in the range  
354 ~~~1000-32000~~ ~3200-32000  $\text{scm}^{-3}$  and ~~~5-4000~~ ~5-4000  $\text{scm}^{-3}$ , respectively, for plumes with  $\sigma_s$  between 10 and 120  
355  $\text{Mm}^{-1}$ . The structure in the scattering profile is generally mirrored in  $dN_{\text{Acc}}$ . The profile of the  
356 aerosol scattering coefficient is mostly correlated to  $dN_{\text{Acc}}$ , and this also reflects the pronounced  
357 spectral variability (i.e., decrease for increasing wavelength) of the scattering coefficient, typical of  
358 pollution/anthropogenic particles.  $dN_{\text{Coarse}}$  also contributes to the scattering signal in some cases  
359 especially at high altitudes (see V16, V20, V21, V22, and V23 above ~2000 m), and this reflects the  
360 low spectral variability of the scattering coefficient. These observations are associated to the dust  
361 intrusion episodes which occurred in the Western Mediterranean basin during TRAQA, which

362 however will not be analysed in detail here. Aerosol layers affected by dust have been labelled with  
363 a “D” in Fig. 6.

364 Maxima of the scattering coefficient have been measured for TRAQA flights V21 and V23 (~120  
365  $\text{Mm}^{-1}$  for pollution\_ in the BL and ~100  $\text{Mm}^{-1}$  in the dust layer), whereas flights V46-V48-V49,  
366 during the first and more polluted phase of SAFMED, are the richest in  $\text{dN}_{\text{Acc}}$  (1500-3000  $\text{scm}^{-3}$   
367 over the whole column). Minima of  $\sigma_s$  and  $\text{dN}_{\text{Acc}}$  are obtained for flight V51 at the beginning of the  
368 second SAFMED phase when clean conditions were observed in the Western Mediterranean.

369 Pollution plumes observed in the different flights extend from the boundary layer to the free  
370 troposphere up to 3000-4000 m altitude. The vertical structure of the aerosol scattering  
371 coefficient/particle concentration is linked to the variability of the atmospheric thermodynamic  
372 structure and is generally characterized by a first layer confined in the MABL (<400 m, profiles  
373 V16, V20, V22, V25, V48, V51), followed by one or more layers within the BL. In the FT pollution  
374 particles occur both as single isolated plumes each about 500-1000 m deep (V21, V24, V25, V30,  
375 V46, V49), or as a more uniform layer extending from the top of the BL up to 2500-4000 m altitude  
376 (V26, V27, V28, V32, V48). The highest values of both the scattering coefficient and  $\text{dN}_{\text{Acc}}$  for  
377 pollution are found within the MABL or BL in most cases, while a local minimum of  $\sigma_s$  and  $\text{dN}_{\text{Acc}}$   
378 is generally identified at the top of the BL. The scattering coefficient and the particle concentration  
379 measured in the FT are comparable with the values observed in the BL, and in few cases even larger  
380 (V25, V26, V30). Only in one case (profile V31)  $\sigma_s$  and  $\text{dN}_{\text{Acc}}$  decrease monotonically with height.  
381 The aerosol vertical distribution, both in the BL and in the FT, often presents a strongly stratified  
382 structure characterized by the presence of several thin sub-layers within one main identified aerosol  
383 plume, as it can be seen in particular in the  $\text{dN}_{\text{Acc}}$  profiles (V20, V21, V22, V25, V46, V49).

384 The particle concentration in the Aitken mode (0.004-0.1  $\mu\text{m}$ ;  $\text{dN}_{\text{Aitken}}$ , not shown in Fig. 6) is  
385 generally below 5000-6000  $\text{scm}^{-3}$  at all altitudes up to 4000 m within pollution plumes.  $\text{dN}_{\text{Aitken}}$  is  
386 correlated with  $\text{dN}_{\text{Acc}}$  in most of the observed cases, which indicates the common source of particles



387 in these two size ranges. Few layers exceeding  $\sim 10000\text{-}15000\text{ scm}^{-3}$  are observed occasionally both  
388 in the BL and in the FT. These will be discussed in more detail in Sect. 5.4.

389 The  $dN_{\text{Acc}}$  and  $dN_{\text{Aitken}}$  measurements within the BL and in the FT over the sea are comparable with  
390 the values measured close to the surface at ~~urban~~-continental sites under pollution conditions ([see](#)  
391 [Table 2](#)) (Petzold et al., 2002; Mallet et al., [2003 and](#) 2005; Weiegner et al., 2006; Junkermann,  
392 2009; Hamburger et al., 2012; [Highwood et al., 2012](#)). This suggests that the export towards the  
393 basin favours the redistribution of the pollution plumes along the vertical. Because of mixing in the  
394 BL, measured concentrations within the BL can be as high as those observed close to the surface  
395 ~~over at urban~~-~~continentals~~-~~site~~-~~under~~-~~pollution~~-~~conditions~~. Values of  $dN$  as high as in the BL are  
396 observed in the FT because of transport in specific conditions, as discussed below.

397 The observations of aerosol profiles obtained during TRAQA and SAFMED are representative of  
398 the complex transport regimes which characterizes the export towards the Western basin and that is  
399 mostly determined by the interaction between regional meteorology and local dynamics (e.g.,  
400 Gangoiti et al., 2001). A first example is associated to the measurements in the area of Barcelona.  
401 As discussed in Pérez et al. (2004) the presence of mountains up to  $\sim 500\text{-}3000$  m altitude a few  
402 kilometres inland favours, during summertime, the recirculation of pollutants along the coasts of  
403 Spain. In these cases, the aerosols emitted at the surface in coastal areas are transported inland and  
404 uplifted by sea breezes and mountain winds then the plumes are re-injected at different altitudes and  
405 distances from the coast. During the TRAQA flights V24, V25, and V26, under the influence of  
406 pollution outflow from the Barcelona area, we detected the presence of aerosol layers with elevated  
407 concentrations ( $dN_{\text{Acc}} \sim 2000\text{-}3000\text{ scm}^{-3}$ ) up to 3500 m altitude at a distance of  $\sim 30$  to 250 km from  
408 the coast of Spain. Another example of complex dynamics linked to coastal orography is that  
409 associated to the export from northern Italy and the Po Valley towards the Gulf of Genoa. The  
410 presence of the Apennine Mountains close to the Ligurian coasts (max elevation  $\sim 1500\text{-}2000$  m)  
411 causes the uplift of continental air masses so determining the injection of aerosol plumes at different

412 altitudes both inside and outside the BL. Examples are given by flights V19, V21 and V52 for  
413 which pollution aerosols from northern Italy are measured up to ~2000-3000 m altitude throughout  
414 the Gulf of Genoa. Finally, another meteorological condition which largely influences the aerosol  
415 export and distribution over the Western Mediterranean is the Mistral/Tramontane wind regime.  
416 Under the influence of the Mistral flow, atmospheric aerosols can be dispersed as far as hundreds of  
417 kilometres over the open sea, as discussed by Salameh et al. (2007). Examples are given in profiles  
418 V20 and V28, performed at more than 100 km from the French coasts, for which pollution layers  
419 associated to a Mistral flow are measured up to 2000-3000 m altitude.

420

## 421 **5.2 Trace gases vertical profiles**

422 Figure 7 shows O<sub>3</sub> versus CO for all TRAQA and SAFMED flights, while examples of CO and O<sub>3</sub>  
423 profiles representatives of different conditions are reported in Fig. 8 and 10.

424 CO and O<sub>3</sub> vary in the range 60-1~~6570~~ ppbv and 30-85 ppbv, respectively. The 25<sup>th</sup> and 75<sup>th</sup>  
425 percentiles are 87 and 105 ppbv for CO and 49 and 62 ppbv for O<sub>3</sub>, representative of moderate  
426 pollution conditions (i.e., Parrish et al., 1998). By comparison, the values measured over land in  
427 central Italy during flight V49 are in the range 80-180 ppbv for carbone monoxide and 40-85 ppbv  
428 for ozone. CO and O<sub>3</sub> are generally correlated (correlation coefficient  $R^2 \sim 0.5-0.8$ ) within measured  
429 pollution plumes, and also correlated with  $\sigma_s$  and  $N_{Acc}$  both in the BL and in the FT, which indicates  
430 photochemically active plumes. CO is generally higher in the BL, and shows absolute maxima in  
431 the lowest levels (V20, V21, V24, V28, V46), then it decreases in the FT. Ozone presents a more  
432 complicated vertical structure due to the different photochemical and dynamical processes which  
433 control its formation and distribution. At first, local peaks of O<sub>3</sub> correlated with CO are observed in  
434 correspondence of pollution plumes both in the BL and in the FT. An absolute maximum of O<sub>3</sub> is  
435 sometimes found near the top of the BL (V24, V25, V30) possibly due to aged air masses trapped in  
436 the boundary layer. Isolated peaks of O<sub>3</sub> (~75-80 ppbv) not correlated with aerosols and CO are also

437 measured in few cases above 3000-3500 m (V21, V25, V27, V28, V52). The analysis of back-  
438 trajectories indicates that these high-altitude ozone layers are associated to the descent of air masses  
439 travelling at about 7-8 km, which thus may suggest a downward transport from the upper  
440 troposphere or the tropopause region due to a stratosphere-troposphere exchange (Ancellet and  
441 Ravetta, 2005). Finally, absolute minima of O<sub>3</sub> (~15-30 ppbv) are measured within the dust layers  
442 during flights V20 and V21, maybe related to the dust/ozone heterogeneous reactions which leads  
443 to O<sub>3</sub> destruction, as documented in several studies (Bonasoni et al., 2004; Haywood et al., 2011).

444

### 445 **5.3 $\Delta O_3/\Delta CO$ and $dN_{Aitken}/dN_{Acc}$ ratios and variability of pollution plume composition**

446 Using the O<sub>3</sub>, CO,  $dN_{Aitken}$  and  $dN_{Acc}$  measurements we have estimated:

- 447 - the O<sub>3</sub>-CO enhancement ratio ( $\Delta O_3/\Delta CO$ ), i.e. the ratio of the ozone to carbon monoxide  
448 variations compared to their baseline values. The  $\Delta O_3/\Delta CO$  enhancement ratio is frequently  
449 used to estimate the efficiency of O<sub>3</sub> formation and its export (Parrish et al., 1993; Zhang et  
450 al., 2006). From our observations (Fig. 7) we have estimated a background value of ~70  
451 ppbv in the BL and 60 ppbv in the FT for CO and ~30 ppbv for O<sub>3</sub> both in the BL and in the  
452 FT.
- 453 - The Aitken to accumulation number ratio ( $dN_{Aitken}/dN_{Acc}$ ), which defines the relative  
454 importance of particles in the Aitken and accumulation modes.  $dN_{Aitken}$  is generally  
455 associated to gas-to-particle conversion and nucleation events and is higher in fresh plumes,  
456 while it decreases with the increasing of the plume lifetime due to coagulation or  
457 condensation of water-soluble chemical species on the particle surface (Kulmala et al.,  
458 2004).

459 The combination of  $\Delta O_3/\Delta CO$  and  $dN_{Aitken}/dN_{Acc}$  has been used to retrieve additional information  
460 on the atmospheric vertical structure, layering, and particle aging.

461 Within detected pollution plumes the  $\Delta\text{CO}$  and  $\Delta\text{O}_3$  reach up to 100-120 ppbv and 45-55 ppbv,  
462 respectively, with a corresponding  $\Delta\text{O}_3/\Delta\text{CO}$  ratio which varies in the range  $\sim 0.10$ -2.0 for all cases.  
463 These values are comparable with the range of observations available in the literature for fresh and  
464 moderately aged pollution plumes in the BL and in the lower FT ( $\sim 0.2$ -1.0) (Chin et al., 1994;  
465 Parrish et al., 1998; Zhang et al., 2006; Cristofanelli et al., 2013).  $dN_{\text{Aitken}}/dN_{\text{Acc}}$  is between about 1  
466 and 20 in most of pollution cases, which indicates the presence of both fresh layers rich in Aitken  
467 particles and aged plumes poor in Aitken particles. Extremely high values of  $dN_{\text{Aitken}}/dN_{\text{Acc}}$  ( $\sim 50$ -  
468 ~~100~~200) are measured in few cases in layers with very low  $dN_{\text{Acc}}$  concentrations.

469 The large variability in  $\Delta\text{O}_3/\Delta\text{CO}$  and  $dN_{\text{Aitken}}/dN_{\text{Acc}}$  indicates a strong heterogeneity in terms of  
470 composition and lifetime for the different observed plumes. This heterogeneity reflects the  
471 complexity in terms of sources, production processes, and transport mechanisms which  
472 characterizes the Western basin. In order to illustrate this point, we have selected three examples  
473 representative of different conditions observed in different areas of the basin: (i) V19, performed in  
474 the Gulf of Genoa in correspondence of continental outflow events from Northern Italy/Po Valley;  
475 (ii) V20, performed in Southern France during a Mistral event; (iii) V24, which measured the export  
476 of pollution from the area of Barcelona. The vertical profiles of the spectral scattering coefficient  $\sigma_s$ ,  
477 temperature T, relative humidity RH,  $dN_{\text{Acc}}$ ,  $dN_{\text{Aitken}}$ , CO,  $\text{O}_3$ ,  $\Delta\text{O}_3/\Delta\text{CO}$ ,  $dN_{\text{Aitken}}/dN_{\text{Acc}}$  and wind  
478 are reported in Fig. 8 for these cases.

479 *1. V19: export from northern Italy/Po Valley.* The profile shown for flight V19 (Fig. 8a) is  
480 characterized by the presence of ~~two~~three different aerosol structures: the first one below 800 m,  
481 characterized by a lower  $dN_{\text{Aitken}}/dN_{\text{Acc}}$  ( $\sim 1$ -5)  ~~$dN_{\text{Aitken}}$~~  and relatively high  ~~$\text{O}_3$  concentrations~~  
482 ~~( $dN_{\text{Aitken}}/dN_{\text{Acc}} \sim 1$ -5,  $\Delta\text{O}_3/\Delta\text{CO}$  ( $\sim 0.4$ -1.5)), possibly associated to moderately aged pollution, and;~~  
483 the second one between 800 and 2600 m, very richer in fine particles ( $dN_{\text{Aitken}}/dN_{\text{Acc}} \sim 5$ -15), so  
484 possibly associated-linked to fresher emissions; and the third one above 2600 m, where the ratio  
485  $dN_{\text{Aitken}}/dN_{\text{Acc}}$  rises rapidly, as will be further discussed in Sect. 5.4. The export of fresh pollution at

486 | ~~high altitudes~~800-2600 m from northern Italy as observed in V19 may be ~~associated~~related to the  
487 | peculiar orography of this region and the uplift of continental air masses. This is confirmed by the  
488 | analysis of the back-trajectories (Fig. 9) which indicates that the air masses arriving at 1000 and  
489 | 2000 m passed over the western Po Valley at an altitude of about 400-1200 m and were then  
490 | uplifted near the Ligurian coast to enter the basin above the BL. Junkermann (2009) measured high  
491 | levels of fine particles up to about 2000 m in the western Po Valley, which means that the altitudes  
492 | of 400-1200 m reached by our investigated air masses could have been sufficient for them to collect  
493 | fresh emitted particles along their path. Conversely, below 800 m the air mass trajectory shows a  
494 | longer subsidence over the sea surface in the troposphere which has possibly favoured the advection  
495 | of more aged plumes, or the mixing with sea salts thus inducing the decrease of the  $dN_{\text{Aitken}}/dN_{\text{Acc}}$   
496 | ratio. It should be noted that the aerosol layer in the FT also shows relatively higher values of the  
497 |  $\Delta O_3/\Delta CO$  ratio ( $\sim 0.6-1.0$ ) compared to the more aged plume in the BL. The enhanced amount of  $O_3$   
498 | in this air mass can be linked to a high concentration of volatile precursors which may have  
499 | favoured the build-up of ozone during the plume evolution. In a recent work, Kaiser et al. (2014)  
500 | suggest that in the Po Valley the high content of formaldehyde, also observed by Junkermann et al.  
501 | (2009), may be responsible for the excess of  $O_3$  production. Fresh layers in the FT up to  $\sim 2000-$   
502 |  $3000$  m possibly associated to pollution export from northern Italy have been also observed during  
503 | flights V21 and V52 (not shown).

504 | 2. V20: export during a Mistral/Tramontane event. V20 provides an example of export during a  
505 | Mistral/Tramontane event. As shown in Fig. 8b, winds from the northwest direction are measured at  
506 | all altitudes during flight V20. The aerosol profile in the BL is characterized in the first  $\sim 400$  m by  
507 | the presence of a layer richer in  ~~$dN_{\text{Aitken}}$  ( $dN_{\text{Aitken}}/dN_{\text{Acc}} > 20$ )~~ and CO (100 ppbv close to the surface;  
508 | ~~CO data not available between 150 and 650 m)~~ ~~and  $dN_{\text{Aitken}}$  ( $dN_{\text{Aitken}}/dN_{\text{Acc}} > 20$ )~~ possibly linked to  
509 | fresh pollution, followed by the alternation of several layers characterized by a variable  $dN_{\text{Aitken}}$   
510 | ( $1000-6000 \text{ cm}^{-3}$ ) and lower CO ( $\sim 70$  ppbv). A local minimum of  $dN_{\text{Aitken}}$  and  $\sigma_s$  is found at  $\sim 400$

511 | m. For all these layers the O<sub>3</sub> is very low (~30-40 ppbv) and the ΔO<sub>3</sub>/ΔCO ratio is <0.6-0.8. At  
512 | higher altitudes, between 1400 and 2000 m, we observe a layer enriched in O<sub>3</sub> (ΔO<sub>3</sub>/ΔCO~1-2) in  
513 | correspondence of an almost aerosol-free region. This enriched ozone layer might be possibly  
514 | associated to a downward transport from higher tropospheric layers, as also suggested by the back-  
515 | trajectories (Fig. 9), as well as to the mixing with ozone rich layers along the air mass trajectory.  
516 | Larger particles, from long-range transport of Saharan dust at latitudes below 30° N, are measured  
517 | between 2000 and 3000 m, with a minimum of O<sub>3</sub> (~15-20 ppbv) registered within the layer.  
518 | Several other flights were performed during Mistral/Tramontane episodes (V27, V28, V30, V32)  
519 | and show, similarly to V20, the presence of several layers both in the BL and the FT.

520 | 3. V24: export from the Barcelona area. Measurements during V24 may be taken as representative  
521 | of local recirculation (Pérez et al., 2004). In the V24 profile in Fig. 8c we may recognize up to 5  
522 | different aerosol layers. A first layer at <200 m within the MABL, coming from the southwest and  
523 | directly exported from the area of Barcelona. The layer is characterized by high CO (90-120 ppbv),  
524 | and relatively low values of dN<sub>Aitken</sub> (~4000 scm<sup>-3</sup>) and O<sub>3</sub> (~50 ppbv), which possibly suggest the  
525 | mixing of pollution with marine particles close to the sea surface. A second layer of fresher  
526 | particles, always coming from the southwestern direction, is observed above the MABL between  
527 | 200 and 600 m (dN<sub>Aitken</sub>~6000-8000 scm<sup>-3</sup>, O<sub>3</sub>~70 ppb, with dN<sub>Aitken</sub>/dN<sub>Acc</sub>~5-15, and  
528 | ΔO<sub>3</sub>/ΔCO~0.8-1.5). A third, more aged, sublayer (dN<sub>Aitken</sub>/dN<sub>Acc</sub>~2-5, ΔO<sub>3</sub>/ΔCO~0.8-1.0) is  
529 | observed within the BL between 600 and 1000 m. The FT is characterized by the presence of  
530 | moderately aged plumes from ~1000 to 2800 m (dN<sub>Aitken</sub>/dN<sub>Acc</sub>~2-10, ΔO<sub>3</sub>/ΔCO~0.2-0.8), and a  
531 | very aged plume at 2800-3800 m almost deprived in Aitken particles and richer in O<sub>3</sub>  
532 | (dN<sub>Aitken</sub>/dN<sub>Acc</sub><1, ΔO<sub>3</sub>/ΔCO~0.6-1.5). A marked local minimum is observed at the top of the BL  
533 | for σ<sub>s</sub>, dN<sub>Acc</sub>, dN<sub>Aitken</sub>, CO, and O<sub>3</sub>, suggesting the presence of air masses with different origin  
534 | between the BL and the FT. This is also confirmed by the analysis of the back-trajectories (Fig. 9)  
535 | which indicates a low level air masses coming from the Spanish coasts in the BL, and air masses

536 travelling at higher altitudes in the FT. In particular, the layer at 2800-3800 m is possibly associated  
537 to an intercontinental transport from Northern America, as shown in the trajectory ending at 3500  
538 m. A similar structure characterized by the alternation of fresher and more aged plumes in the BL  
539 and FT is also observed in V25 for which aerosol layers are detected up to 4000 m altitude.

540 The detailed analysis of these three events evidences the complexity of the atmospheric structure  
541 over the Western Mediterranean basin in link with the different dynamical processes involved.

542

#### 543 **5.4 Layers with enhanced Aitken mode particle numbers**

544 Isolated layers with  $dN_{\text{Aitken}} \sim 10000-15000 \text{ scm}^{-3}$  have been observed ~~in few cases~~ occasionally both  
545 in the BL and in the FT. The vertical profiles of  $dN_{\text{Aitken}}$  ~~only~~ for some selected cases are shown in  
546 Fig. 10.

547 For about half of the observed events (~~V16 at ~200-400 m, V21 at ~400-800 m, V28 at ~250 m, and~~  
548 ~~V31 at ~1000-3000 m; only V28 and V31 shown in Fig. 10~~) the  $dN_{\text{Aitken}}$  layer ~~presents a good~~  
549 ~~correlation~~ appears related ~~with~~ to a simultaneous increase in  $dN_{\text{Acc}}$ , CO, and  $O_3$ , which suggests  
550 that the layer has been transported from a region directly emitting in this size range. These cases  
551 are: V16 at ~200-400 m, V21 at ~400-800 m, V28 at ~250 m, and V31 at ~1000-3000 m (only V28  
552 and V31 are shown in Fig. 10). The most remarkable example is ~~The most remarkable example is~~  
553 V31 (Fig. 10a), performed close to the coasts of Spain near Valencia, for which ~~for which~~ the high  
554  $dN_{\text{Aitken}}$  layer extends from the top of the BL to ~3000 m altitude. The wind vector and the back-  
555 trajectories (not shown) indicates that the air mass comes from the western-southwestern direction  
556 above 1000 m, so the  $dN_{\text{Aitken}}$  layer can be directly related to pollution export from the urban region  
557 of Valencia.

558 ~~In~~ In all the other cases the high  $dN_{\text{Aitken}}$  layer ~~appears~~ is generally not related to simultaneous  $dN_{\text{Acc}}$   
559 and  $O_3$  increase. Two of these cases (V16 at ~800-1000 m and V28 at ~100 m) occur in the BL.

560 For the V28 layer (Fig. 10b) the  $dN_{\text{Aitken}}$  is correlated with CO which might indicate the influence of  
561 local emissions close to the surface level (i.e., ship emissions). CO values are relatively high (140-  
562 160 ppbv) within the layer. It has been often assumed that new particle formation events (NPF) only  
563 occur in almost clean environments (e.g., O'Dowd et al., 2010; Sellegri et al., 2010), and that they  
564 are suppressed under polluted conditions. In a recent study, Brines et al. (2014) show the occurrence  
565 of NPF events also in urban areas with high level of pollution in the Mediterranean region. So, we  
566 explore the possibility of NPF in our observations. Given the size ranges of the CPC and PCASP,  
567 however, we cannot discriminate within  $dN_{\text{Aitken}}$  the particle concentration in the sole 4-20 nm  
568 range, i.e. the size range involved in nucleation. So it is not possible to directly associate the V28  
569 observations to NPF. In order to obtain a qualitative indication of the possible occurrence of NPF,  
570 we have looked at the air mass dynamics within the layer. Several studies suggest, in fact, that NPF  
571 might be favoured by turbulence and air mass mixing (e.g., Nilsson et al., 2001; Wehner et al.,  
572 2010). We have thus looked at the gradient Richardson number (Ri) which gives information on the  
573 atmospheric dynamical stability. Vertical profiles of Ri are also shown in Fig. 10. For V28 the  
574 vertical profile of Ri indicates that below 200 m the Ri number is consistently below zero, which  
575 suggests well established turbulent conditions possibly favouring NPF in this layer.

576 In other two cases (V19, Fig. 10c, and V26, Fig. 10d), under lower pollution conditions ( $\text{CO} < 100$ ),  
577 we measured high  $dN_{\text{Aitken}}$  concentration in correspondence of low  $dN_{\text{Acc}}$  layers in the FT at ~2800-  
578 3000 m for V19 and 3500-4500 m for V26. For V19 and V26 layers,  $dN_{\text{Aitken}}$  seems anticorrelated  
579 to CO. Also in this case the Richardson number is below  $Ri_{\text{crit}}$  in correspondence of the Aitken peak  
580 meaning that conditions are favorable for turbulence within the layer, and this may indicate also in  
581 this case the possible role of NPF.

582 Finally, a case of high  $dN_{\text{Aitken}}$  concentration has been also observed in correspondence of dust  
583 particles between ~3000 and 4000 m (V23b, Fig. 10e). This layer can be possibly linked to the



584 photochemically-induced nucleation which may occur in presence of dust and SO<sub>2</sub> as hypothesised  
585 in a recent study by Dupart et al. (2012) and observed by Nie et al. (2014).

586

## 587 **6. Conclusions**

588 The data presented in this paper gives an overview of the distribution of aerosols and trace gases  
589 within the tropospheric column up to 5000 m above the Western Mediterranean basin.

590 These data add to the very few available measurements of aerosol and trace gases vertical profiles  
591 over the sea surface in the Central (e.g., Junkermann, 2001; Meloni et al., 2003; Di Iorio et al.,  
592 2003; Pace et al., 2014) and Eastern (e.g., Formenti et al., 2002; Dulac and Chazette, 2003) parts of  
593 the basin thus contributing to improve the description of the atmospheric composition and structure  
594 over the whole Mediterranean area.

595 Observations from the present study indicate that continental pollution strongly affects the  
596 composition and structure of the Western Mediterranean basin both close to coastal regions and in  
597 the open sea. Pollution layers extend up to 250 km far from the coasts and reach up to 3000-4000 m  
598 altitude, presenting a complex and highly stratified structure. The measured particle concentration is  
599 comparable with the values reported for continental Europe (Petzold et al., 2002; Junkermann,  
600 2009; Hamburger et al., 2012). ~~In addition, the geographical distribution of aerosols and trace gases  
601 observed in this study appears quite homogeneous within the investigated area, suggesting a  
602 relatively similar contribution from the various sources located around the north-western basin.~~

603 Pollution plumes with different compositions, origins, and lifetimes are observed in link with the  
604 different observed dynamical export conditions and meteorological regimes. The aerosol and trace  
605 gas observations during TRAQA and SAFMED are consistent with the results of former campaigns  
606 and with the interpretation of observed or well known air-masses dynamics and meteorological

607 phenomena that can occur in the Western basin (Flamant and Pelon, 1996; Millan et al., 1997;  
608 Gangoiti et al., 2001; Pérez et al., 2004; Mallet et al., 2005).

609 The large heterogeneity in aerosol compositions, origins, and lifetimes as documented in this study  
610 can reflect in a large heterogeneity of aerosol optical properties, with consequences for their direct  
611 radiative effect in this part of the basin. This aspect will be investigated in a companion paper  
612 analysing the TRAQA and SAFMED in situ measurements of the aerosol absorption and scattering  
613 properties and their variability.

614 From the present observations, it is also interesting to note the relatively high values of  $dN_{\text{Aitken}}$   
615 measured both in the BL and the FT, which evidences the important contribution of ultrafine  
616 particles at all altitudes over the basin. These can be linked to the different export mechanisms  
617 previously discussed, as well as the possible occurrence of NPF events. Aitken particle profiles are  
618 very rare over the sea surface in the Mediterranean (e.g., Junkermann et al. 2001; Pace et al.,  
619 [2014](#)[2015](#)) and data comparison is quite difficult. Few studies have observed NPF in the FT in  
620 continental areas (Boulon et al., 2010; Rose et al., 2014) and suggest that the export of pollution  
621 into the upper troposphere, as it is common in the Western basin, might promote the occurrence of  
622 these events. The observations of the present study may thus also have very large implications due  
623 to the crucial role of NPF in controlling the atmospheric cloud condensation nuclei concentration  
624 (Spracklen et al., 2008) and the associated aerosol indirect effect on climate.

625

## 626 **Author contributions**

627 J.-L.A., F.R., G.A., M.B., A.B., P.F. and K.S. designed the TRAQA and SAFMED experiments and  
628 coordinated the campaigns. C.G., N.G., and C.D.B operated the instruments on board the ATR-42  
629 during the flights. C.D.B. performed the data analysis with contributions from L.D., P.F., F.R.,  
630 A.B., G.A., J.-C.R., and M.B.. G.A. performed the FLEXTRA simulations. J.-C.R. performed the  
631 WRF-Chem simulations. C.D.B. wrote the manuscript.

632

## 633 **Acknowledgements**

634 All measurement presented here are from the Chemistry-Aerosol Mediterranean Experiment project  
635 (ChArMEx, <http://charmex.lsce.ipsl.fr>), which is the atmospheric component of the French  
636 multidisciplinary program MISTRALS (Mediterranean Integrated Studies at Regional And Local  
637 Scales). ChArMEx-France was principally funded by INSU, ADEME, ANR, CNES, CTC (Corsica  
638 region), EU/FEDER, Météo-France, and CEA. TRAQA was funded by ADEME/PRIMEQUAL and  
639 MISTRALS/ChArMEx programmes and Observatoire Midi-Pyrénées. SAFMED was funded by the  
640 ANR project SAF-MED (Secondary Aerosol Formation in the MEDiterranean, [grant SIMI6 ANR-  
641 12-BS06-0013](#)). C. Di Biagio thanks the Centre National des Etudes Spatiales (CNES) for financial  
642 support.

643 The authors wish to thank the technicians, pilots and ground crew of SAFIRE (Service des Avions  
644 Français Instruments pour la Recherche en Environnement) for facilitating the instrument  
645 integration and conducting flying operations. We thank S. Chevaillier, L. Girault, R. Loisil, J.  
646 Pelon, S. Triquet, and P. Zapf for their contribution during the campaigns. We thank S. Basart, J.  
647 M. Baldasano, M. Mallet, P. Goloub, J. Piazzola and their staff for establishing and maintaining the  
648 Barcelona, Ersa, and Frioul AERONET sites. Helpful discussions with G. Pace are gratefully  
649 acknowledged.

650 [We thank also two anonymous reviewers whose suggestions helped to clarify the manuscript.](#)

651

## 652 **References**

- 653 Ancellet, G. and Ravetta, F.: Analysis and validation of ozone variability observed by lidar during  
654 the ESCOMPTE-2001 campaign, *Atmos. Res.*, 74, 435–459, 2005.
- 655 Anderson, T. L., Covert, D. S., Marshall, S. F., Laucks, M. L., Charlson, R. J., Waggoner, A. P.,  
656 Ogren, J. A., Caldow, R., Holm, R. L., Quant, F. R., Sem, G. J., Wiedensholer, A., Ahlquist, N.  
657 A., and Bates, T. S.: Performance characteristics of a high-sensitivity, three-wavelength, total  
658 scatter/backscatter nephelometer, *J. Atmos. Ocean. Tech.*, 13, 967–986, 1996.

- 659 Anderson, T. L. and Ogren, J. A.: Determining aerosol radiative properties using the TSI 3563  
660 integrating nephelometer, *Aerosol Sci. Technol.*, 29, 57–69, 1998.
- 661 Bonasoni, P., Cristofanelli, P., Calzolari, F., Bonafè, U., Evangelisti, F., Stohl, A., Zauli Sajani, S.,  
662 van Dingenen, R., Colombo, T., and Balkanski, Y.: Aerosol-ozone correlations during dust  
663 transport episodes, *Atmos. Chem. Phys.*, 4, 1201-1215, doi:10.5194/acp-4-1201-2004, 2004.
- 664 Boucher, O., Randall, D., Artaxo, P., Bretherton, C., Feingold, G., Forster, P., Kerminen, V.-M.,  
665 Kondo, Y., Liao, H., Lohmann, U., Rasch, P., Satheesh, S. K., Sherwood, S., Stevens, B., and  
666 Zhang, X. Y.: Clouds and Aerosols. In: *Climate Change 2013: The Physical Science Basis. Contribution of Working Group I to the Fifth Assessment Report of the Intergovernmental Panel on Climate Change* [Stocker, T.F., D. Qin, G.-K. Plattner, M. Tignor, S.K. Allen, J. Boschung, A. Nauels, Y. Xia, V. Bex and P.M. Midgley (eds.)]. Cambridge University Press, Cambridge, United Kingdom and New York, NY, USA, 571-657, 2013.
- 671 Boulon, J., Sellegri, K., Venzac, H., Picard, D., Weingartner, E., Wehrle, G., Collaud Coen, M.,  
672 Bütikofer, R., Flückiger, E., Baltensperger, U., and Laj, P.: New particle formation and ultrafine  
673 charged aerosol climatology at a high altitude site in the Alps (Jungfraujoch, 3580 m a.s.l.,  
674 Switzerland), *Atmos. Chem. Phys.*, 10, 9333–9349, doi: 10.5194/acp-10-9333-2010, 2010.
- 675 Brines, M., Dall'Osto, M., Beddows, D. C. S., Harrison, R. M., Gómez-Moreno, F., Núñez, L.,  
676 Artíñano, B., Costabile, F., Gobbi, G. P., Salimi, F., Morawska, L., Sioutas, C., and Querol, X.:  
677 Frequency of new particle formation events in the urban Mediterranean climate, *Atmos. Chem. Phys. Discuss.*, 14, 26463-26494, doi:10.5194/acpd-14-26463-2014, 2014.
- 679 Chazette, P., Randriamiarisoa, H., Sanak, J., Couvert, P., and Flamant, C.: Optical properties of  
680 urban aerosol from airborne and ground based in situ measurements performed during the  
681 ESQUIF program, *J. Geophys. Res.*, 110, D02206, doi:10.1029/2004JD004810, 2005.
- 682 Chin, M., Jacob, D. J., Munger, J. W., Parrish, D. D., and Doddridge, B. G.: Relationship of ozone  
683 and carbon monoxide over North America, *J. Geophys. Res.*, 99, 14,565–14,573, 1994.
- 684 Colette, A., Ancellet, G., Menut, L., and Arnold, S. R.: A Lagrangian analysis of the impact of  
685 transport and transformation on the ozone stratification observed in the free troposphere during  
686 the ESCOMPTE campaign, *Atmos. Chem. Phys.*, 6, 3487-3503, doi:10.5194/acp-6-3487-2006,  
687 2006.
- 688 Cristofanelli, P., Fierli, F., Marinoni, A., Calzolari, F., Duchi, R., Burkhart, J., Stohl, A., Maione,  
689 M., Arduini, J., and Bonasoni, P.: Influence of biomass burning and anthropogenic emissions on  
690 ozone, carbon monoxide and black carbon at the Mt. Cimone GAW-WMO global station (Italy,  
691 2165 m a.s.l.), *Atmos. Chem. Phys.*, 13, 15–30, 2013.
- 692 Di Iorio, T., di Sarra, A., Junkermann, W., Cacciani, M., Fiocco, G., and Fua`, D.: Tropospheric  
693 aerosols in the Mediterranean: 1. Microphysical and optical properties, *J. Geophys. Res.*,  
694 108(D10), 4316, doi:10.1029/2002JD002815, 2003.
- 695 Drobinski, P, Saïd, F., Ancellet, G., Arteta, J. Augustin, P., Bastin, S., Brut, A., Caccia, J. L.,  
696 Campistron, B., Cautenet, S., Colette, A., Coll, I., Corsmeier, U., Cros, B., Dabas, A., Delbarre,  
697 H., Dufour, A., Durand, P., Guénard, V., Hasel, M., Kalthoff, N., Kottmeier, C., Lasry, F.,  
698 Lemonsu, A., Lohou, F., Masson, V., Menut, L., Moppert, C., Peuch, V. H., Puygrenier, V.,  
699 Reitebuch, O., and Vautard, R.: Regional transport and dilution during high-pollution episodes in  
700 southern France: Summary of findings from the Field Experiment to Constraint Models of  
701 Atmospheric Pollution and Emissions Transport (ESCOMPTE), *J. Geophys. Res.*, 112, D13105,  
702 doi:10.1029/2006JD007494, 2007.

- 703 Dulac, F., and Chazette, P.: Airborne study of a multi-layer aerosol structure in the eastern  
704 Mediterranean observed with the airborne polarized lidar ALEX during a STAAARTE campaign  
705 (7 June 1997), *Atmos. Chem. Phys.*, 3, 1817–1831, doi:10.5194/acp-3-1817-2003, 2003.
- 706 Dupart, Y.; King, S. M., Nekat, B., Nowak, A., Wiedensohler, A., Herrmann, H., David, G.,  
707 Thomas, B., Miffre, A., Rairoux, P., D'Anna, B., and George, C.: Mineral dust photochemistry  
708 induces nucleation events in the presence of SO<sub>2</sub>. *PNAS*, 109, (51), 20842–20847, 2012.
- 709 Ebert, M., Weinbruch, S., Rausch, A., Gorzawski, G., Hoffmann, P., Wex, H., and Helas, G.: The  
710 complex refractive index of aerosols during LACE 98 as derived from the analysis of individual  
711 particles, *J. Geophys. Res.*, 107, D21, 8121, doi:10.1029/2000JD000195, 2002.
- 712 Ebert, M., Weinbruch, S., Hoffmann, P., and Ortner, H. M.: The chemical composition and complex  
713 refractive index of rural and urban influenced aerosols determined by individual particle  
714 analysis, *Atmos. Environ.*, 38, 6531–6545, 2004.
- 715 Flamant, C., and Pelon, J.: Atmospheric boundary-layer structure over the Mediterranean during a  
716 Tramontane event, *Quart. J. Roy. Meteorol. Soc.*, 122, 1741–1778, 1996.
- 717 Formenti, P., Reiner, T., Sprung, D., Andreae, M. O., Wendisch, M., Wex, H., Kindred, D., Dewey,  
718 K., Kent, J., Tzortziou, M., Vasaras, A., and Zerefos, C.: STAAARTE-MED 1998 summer  
719 airborne measurements over the Aegean Sea, 1, Aerosol particles and trace gases, *J. Geophys.*  
720 *Res.*, 107, D21, doi:10.1029/2001JD001337, 2002.
- 721 Formenti, P., Rajot, J. L., Desboeufs, K., Saïd, F., Grand, N., Chevaillier, S., and Schmechtig, C.:  
722 Airborne observations of mineral dust over western Africa in the summer Monsoon season:  
723 spatial and vertical variability of physico-chemical and optical properties, *Atmos. Chem. Phys.*,  
724 11, 6387–6410, doi:10.5194/acp-11-6387-2011, 2011.
- 725 Gangoiti, G., M. M. Millán, R. Salvador, E. Mantilla: Long-Range transport and recirculation of  
726 pollutants in the Western Mediterranean during the RECAPMA Project. *Atmos. Environ.*, 35,  
727 6267–6276, 2001.
- 728 Gkikas, A., Houssos, E. E., Hatzianastassiou, N., Papadimas, C. D., and Bartzokas, A.: Synoptic  
729 conditions favouring the occurrence of aerosol episodes over the broader Mediterranean basin,  
730 *Q. J. R. Meteorol. Soc.*, 138: 932–949. doi:10.1002/qj.978, 2012.
- 731 Grell, G. A., Peckham, S. E., Schmitz, R., McKeen, S. A., Frost, G., Skamarock, W. C., and Eder,  
732 B.: Fully coupled “online” chemistry within the WRF model, *Atmos. Environ.*, 39, 6957–6975,  
733 2005.
- 734 Hamburger, T., McMeeking, G., Minikin, A., Petzold, A., Coe, H., and Krejci, R.: Airborne  
735 observations of aerosol microphysical properties and particle ageing processes in the troposphere  
736 above Europe, *Atmos. Chem. Phys.*, 12, 11533–11554, doi:10.5194/acp-12-11533-2012, 2012.
- 737 Haywood, J., Johnson, B., Osborne, S., Mulcahy, J., Brooks, M., Harrison, M., Milton, S., and  
738 Brindley, H.: Observations and modelling of the solar and terrestrial radiative effects of Saharan  
739 dust: a radiative closure case-study over oceans during the GERBILS campaign, *Q. J. R.*  
740 *Meteorol. Soc.*, 137, 1211–1226, doi:10.1002/qj.770, 2011.
- 741
- 742 [Highwood, E. J., Northway, M. J., McMeeking, G. R., Morgan, W. T., Liu, D., Osborne, S.,](#)  
743 [Bower, K., Coe, H., Ryder, C., and Williams, P.: Aerosol scattering and absorption during the](#)  
744 [EUCAARI-LONGREX flights of the Facility for Airborne Atmospheric Measurements \(FAAM\)](#)  
745 [BAe-146: can measurements and models agree?, \*Atmos. Chem. Phys.\*, 12, 7251–7267,](#)  
746 [doi:10.5194/acp-12-7251-2012, 2012.](#)

- 747 [Holben, B. N., Eck, T. F., Slutsker, I., Tanré, D., Buis, J. P., Setzer, A., Vermote, E., Reagan, J. A.,](#)  
748 [Kaufman, Y., Nakajima, T., Lavenu, F., Jankowiak, I., and Smirnov, A.: AERONET: a federated](#)  
749 [instrument network and data archive for aerosol characterization, \*Rem. Sens. Environ.\*, 66, 1–16,](#)  
750 [1998.](#)
- 751 Jiménez, P., Pérez, C., Rodríguez, A., and Baldasano, J. M. : Correlated levels of particulate matter  
752 and ozone in the western Mediterranean basin: Air quality and lidar measurements, 22<sup>nd</sup> Annual  
753 Conference Am. Assoc. for Aerosol Res., Anaheim, California, 20-24 October 20-24 2003,  
754 2003.
- 755 Jiménez, P., Lelieveld, J., and Baldasano, J. M.: Multiscale modeling of air pollutants dynamics in  
756 the northwestern Mediterranean basin during a typical summertime episode, *J. Geophys. Res.*,  
757 111, D18306, doi:10.1029/2005JD006516, 2006.
- 758 Jiménez-Guerrero, P., Jorba, O., Baldasano, J. M., and Gassó, S.: The use of a modelling system as  
759 a tool for air quality management: Annual high-resolution simulations and evaluation, *Sci. Tot.*  
760 *Environ.*, 390, 323–340, 2008.
- 761 Junkermann, W.: An ultralight aircraft as platform for research in the lower troposphere: System  
762 performance and first results from radiation transfer studies in stratiform aerosol layers and  
763 broken cloud conditions, *J. Atmos. Oceanic Technol.*, 18, 934–946, 2001.
- 764 Junkermann, W.: On the distribution of formaldehyde in the western Po-Valley, Italy, during 800  
765 FORMAT 2002/2003, *Atmos. Chem. Phys.*, 9, 9187-9196, doi:10.5194/acp-9-9187-2009, 2009.
- 766 Kaiser, J., Wolfe, G. M., Bohn, B., Broch, S., Fuchs, H., Ganzeveld, L. N., Gomm, S., Häsel, R.,  
767 Hofzumahaus, A., Holland, F., Jäger, J., Li, X., Lohse, I., Lu, K., Rohrer, F., Wegener, R.,  
768 Mentel, T. F., Kiendler-Scharr, A., Wahner, A., and Keutsch, F. N.: Evidence for an unidentified  
769 ground-level source of formaldehyde in the Po Valley with potential implications for ozone  
770 production, *Atmos. Chem. Phys. Discuss.*, 14, 25139-25165, doi:10.5194/acpd-14-25139-2014,  
771 2014.
- 772 Kallos, G., Astitha, M., Katsafados, P., and Spyrou, C.: Long-range transport of anthropogenically  
773 and naturally produced particulate matter in the Mediterranean and North Atlantic: Current state  
774 of knowledge, *J. Appl. Meteorol. Climatol.*, 46, 1230–1251, 2007.
- 775 Kulmala, M., Vehkamäki, H., Petaja, T., Dal Maso, M., Lauri, A., Kerminen, V.-M., Birmili, W.,  
776 and McMurry, P.H.: Formation and growth rates of ultrafine atmospheric particles: A review of  
777 observations, *J. Aerosol Sci.*, 35(2), 143–176, 2004.
- 778 Lelieveld, J., Berresheim, H., Borrmann, S., Crutzen, P. J., Dentener, F. J., Fischer, H., Feichter, J.,  
779 Flatau, P. J., Heland, J., Holzinger, R., Kormann, R., Lawrence, M. G., Levin, Z., Markowicz,  
780 K. M., Mihalopoulos, N.; Minikin, A., Ramanathan, V., de Reus, M., Roelofs, G. J., Scheeren,  
781 H. A., Sciare, J., Schlager, H., Schultz, M., Siegmund, P., Steil, B., Stephanou, E. G., Stier, P.,  
782 Traub, M., Warneke, C., Williams, J., and Ziereis H.: Global air pollution crossroads over the  
783 Mediterranean, *Science*, 298, 794–799, doi:10.1126/science.1075457, 2002.
- 784 Liu, Y. and Daum, P.: The effect of refractive index on size distributions and light scattering  
785 coefficients derived from optical particle counters, *J. Aerosol Sci.*, 31, 945–957, 2000.
- 786 Mallet, M., Roger, J. C., Despiou, S., Dubovik, O., and Putaud, J. P.: Microphysical and optical  
787 properties of aerosol particles in urban zone during ESCOMPTE, *Atmos. Res.*, 69, 73–97, 15  
788 2003.
- 789 Mallet, M., Van Dingenen, R., Roger, J. C., Despiou, S., and Cachier, H.: In situ airborne  
790 measurements of aerosol optical properties during photochemical pollution events, *J. Geophys.*  
791 *Res.*, 110, D03205, doi:10.1029/2004JD005139, 2005.



- 792 Mallet, M., Gomes, L., Solmon, F., Sellegri, K., Pont, V., Roger, J. C., Missamou, T., and Piazzola,  
793 J.: Calculation of key optical properties of the main anthropogenic aerosols over the Western  
794 French coastal Mediterranean Sea, *Atmos. Res.*, 101, 396–411, 2011.
- 795 Meloni, D., di Sarra, A., DeLuisi, J., Di Iorio, T., Fiocco, G., Junkermann, W., and Pace, G.:  
796 Tropospheric aerosols in the Mediterranean: 2. Radiative effects through model simulations and  
797 measurements, *J. Geophys. Res.*, 108(D10), 4317, doi:10.1029/2002JD002807, 2003.
- 798 Millán, M., Salvador, R., Mantilla, E., and Artinãno, B.: Meteorology and photochemical air  
799 pollution in Southern Europe: experimental results from EC research projects, *Atmos. Environ.*,  
800 30 (12), 1909–1924, 1996.
- 801 Millan, M. M., Salvador, R., Mantilla, E., and Kallos, G.: Photooxidant dynamics in the Western  
802 Mediterranean in summer: Results from European research projects, *J. Geophys. Res.*, 102(D7),  
803 8811–8823, 1997.
- 804 Millán, M. M., Mantilla, E., Salvador, R., Carratala, A., Sanz, M. J., Alonso, L., Gangoiti, G., and  
805 Navazo, M.: Ozone cycles in the western Mediterranean basin: interpretation of monitoring data  
806 in complex terrain, *J. Appl. Meteorol.*, 4, 487–507, 2000.
- 807 Monks, P., Granier, C., Fuzzi, S., Stohl, A., Williams, M., Akimoto, H., Amann, M., Baklanov, A.,  
808 Baltensperger, U., Bey, I., Blake, N., Blake, R., Carslaw, K., Cooper, O., Dentener, F., Fowler,  
809 D., Fragkou, E., Frost, G., Generoso, S., Ginoux, P., Grewe, V., Guenther, A., Hansson, H.,  
810 Henne, S., Hjorth, J., Hofzumahaus, A., Huntrieser, H., Isaksen, I., Jenkin, M., Kaiser, J.,  
811 Kanakidou, M., Klimont, Z., Kulmala, M., Laj, P., Lawrence, M., Lee, J., Liousse, C., Maione,  
812 M., McFiggans, G., Metzger, A., Mieville, A., Moussiopoulos, N., Orlando, J., O’Dowd, C.,  
813 Palmer, P., Parrish, D., Petzold, A., Platt, U., Pöschl, U., Prévôt, A., Reeves, C., Reimann, S.,  
814 Rudich, Y., Sellegri, K., Steinbrecher, R., Simpson, D., ten Brink, H., Theloke, J., van der Werf,  
815 G., Vautard, R., Vestreng, V., Vlachokostas, C., and von Glasow, R.: Atmospheric composition  
816 change – global and regional air quality, *Atmos. Environ.*, 43, 5268–5350,  
817 doi:10.1016/j.atmosenv.2009.08.021, 2009.
- 818 Müller, D., Ansmann, A., Wagner, F., Franke, K., and Althausen, D.: European pollution outbreaks  
819 during ACE 2: Microphysical particle properties and single-scattering albedo inferred from  
820 multiwavelength lidar observations, *J. Geophys. Res.*, 107, D15, 4248, 10.1029/2001JD001110,  
821 2002.
- 822 Nedélec, P., Cammas, J.-P., Thouret, V., Athier, G., Cousin, J.-M., Legrand, C., Abonnel, C.,  
823 Lecoœur, F., Cayez, G., and Marizy, C.: An improved infrared carbon monoxide analyser for  
824 routine measurements aboard commercial Airbus aircraft: technical validation and first scientific  
825 results of the MOZAIC III programme, *Atmos. Chem. Phys.*, 3, 1551–1564, doi:10.5194/acp-3-  
826 1551-2003, 2003.
- 827 Nie, W., Ding, A., Wang, T., Kerminen, V.-M., George, C., Xue, L., Wang, W., Zhang, Q., Petaja,  
828 T., Qi, X., Gao, X., Wang, X., Yang, X., Fu, C., and Kulmala, M.: Polluted dust promotes new  
829 particle formation and growth, *Sci. Rep.*, 4, 6634, doi:10.1038/srep06634, 2014.
- 830 Nilsson, E. D., Rannik, U., Kulmala, M., Buzorius, G., and O’Dowd, C. D.: Effects of continental  
831 boundary layer evolution, convection, turbulence and entrainment, on aerosol formation,  
832 *TellusB*, 53, 441–461, 2001.
- 833 O’Dowd, C., Monahan, C., and Dall’Osto, M.: On the occurrence of open ocean particle production  
834 and growth events, *Geophys. Res. Lett.*, 37, L19805, doi:10.1029/2010GL044679, 2010.
- 835 Pace, G., di Sarra, A., Meloni, D., Piacentino, S., and Chamard, P.: Aerosol optical properties at  
836 Lampedusa (Central Mediterranean). 1. Influence of transport and identification of different  
837 aerosol types, *Atmos. Chem. Phys.*, 6, 697–713, doi:10.5194/acp-6-697-2006.

- 838 Pace, G., Junkermann, W., Vitali, L., di Sarra, A., Meloni, D., Cacciani, M., Cremona, G.,  
839 Iannarelli, A. M., and Zanini, G: On the complexity of the boundary layer structure and aerosol  
840 vertical distribution in the coastal Mediterranean regions: a sea breeze, desert dust transport, and  
841 free-tropospheric air intrusion case study in Southern, submitted to TellusB, [20142015](#).
- 842 Parrish, D. D., Holloway, J. S., Trainer, M., Murphy, P. C., Fehsenfeld, F. C., and Forbes, G. L.:  
843 Export of North America ozone pollution to the North Atlantic Ocean, *Science*, 259, 1436–1439,  
844 1993.
- 845 Parrish, D. D., Trainer, M., Holloway, J. S., Yee, J. E., Warshawsky, M. S., Fehsenfeld, F. C.,  
846 Forbes, G. L., and Moody, J. L.: Relationships between ozone and carbon monoxide at surface  
847 sites in the North Atlantic region, *J. Geophys. Res.*, 103, 13,357– 13,376, 1998.
- 848 Pérez, C., Sicard, M., Jorba, O., Comeron, A., and Baldasano, J. M.: Summertime re-recirculations  
849 of air pollutants over the North-Eastern Iberian coast observed from systematic EARLINET lidar  
850 measurements in Barcelona, *Atmos. Environ.*, 38, 3983–4000, 2004.
- 851 Pérez, N., Pey, J., Castillo, S., Viana, M., Alastuey, A., and Querol, X.: Interpretation of the  
852 variability of levels of regional background aerosols in the Western Mediterranean, *Sci. Tot.*  
853 *Environ.*, 407, 527–540, 2008.
- 854 Petzold, A., Fiebig, M., Flentje, H., Keil, A., Leiterer, U., Schroder, F., Stifter, A., Wendisch, M.,  
855 and Wendling, P.: Vertical variability of aerosol properties observed at a continental site during  
856 the Lindenberg Aerosol Characterization Experiment (LACE 98), *J. Geophys. Res.*, 107, 8128,  
857 doi:10.1029/2001JD001043, 2002.
- 858 Pey, J., Querol, X., and Alastuey, A.: Discriminating the regional and urban contributions in the  
859 North-Western Mediterranean: PM levels and composition, *Atmos Environ*, 44, 1587–96, 2010.
- 860 Raut, J.-C., and Chazette, P.: Vertical profiles of urban aerosol complex refractive index in the  
861 frame of ESQUIF airborne measurements, *Atmos. Chem. Phys.*, 8, 901–919, 2008.
- 862 Rose, C., Sellegri, K., Asmi, E., Hervo, M., Freney, E., Junninen, H., Duplissy, J., Sipilä, M.,  
863 Kontkanen, J., Lehtipalo, K., and Kulmala, M.: Major contribution of neutral clusters to new  
864 particle formation in the free troposphere, *Atmos. Chem. Phys. Discuss.*, 14, 18355–18388,  
865 2014.
- 866 Salameh, T., Drobinski, P., Menut, L., Bessagnet, B., Flamant, C., Hodzic, A., and Vautard, R.:  
867 Aerosol distribution over the western Mediterranean basin during a Tramontane/Mistral event,  
868 *Ann. Geophys.*, 25, 2271–2291, 2007.
- 869 Sellegri, K., Laj, P., Venzac, H., Boulon, J., Picard, D., Villani, P., Bonasoni, P., Marinoni, A.,  
870 Cristofanelli, P., and Vuillermoz, E.: Seasonal variations of aerosol size distributions based on  
871 long-term measurements at the high altitude Himalayan site of Nepal Climate Observatory-  
872 Pyramid (5079 m), Nepal, *Atmos. Chem. Phys.*, 10, 10679–10690, doi:10.5194/acp-10-10679-  
873 2010, 2010.
- 874 Soriano, C., Baldasano, J. M., Buttler, W. T., and Moore, K.: Circulatory patterns of air pollutants  
875 within the Barcelona air basin in a summertime situation: lidar and numerical approaches.  
876 *Bound.-Lay. Meteorol.*, 98 (1), 33–55, 2001.
- 877 Spracklen, D. V., Carslaw, K. S., Kulmala, M., Kerminen, V.-M., Sihto, S.-L., Riipinen, I.,  
878 Merikanto, J., Mann, G. W., Chipperfield, M. P., and Wiedensohler, A.: Contribution of particle  
879 formation to global cloud condensation nuclei concentrations, *Geophys. Res. Lett.*, 35, L06808,  
880 doi:10.1029/2007GL033038, 2008.



881 Stohl, A., Wotawa, G., Seibert, P., and Krompkolb, H.: Interpolation errors in wind fields as a  
882 function of spatial and temporal resolution and their impact on different types of kinematic  
883 trajectories, *J. Appl. Meteorol.*, 34, 2149–2165, 1995.

884 Velchev, K., Cavalli, F., Hjorth, J., Marmer, E., Vignati, E., Dentener, F., and Raes, F.: Ozone over  
885 the Western Mediterranean Sea – results from two years of shipborne measurements, *Atmos.*  
886 *Chem. Phys.*, 11, 675-688, doi:10.5194/acp-11-675-2011, 2011.

887 Wallace J.M., and Hobbs, P.V.: *Atmospheric science: an introductory survey* (2nd edition).  
888 International Geophysics Series 92, Academic press, Burlington, 484pp, 2006.

889 Wehner, B., H. Siebert, A. Ansmann, F. Ditas, P. Seifert, F. Stratmann, A. Wiedensohler, A. 956  
890 Apituley, R. A. Shaw, H. E. Manninen, and M. Kulmala (2010), Observations of turbulence  
891 induced new particle formation in the residual layer, *Atmos. Chem. Phys.*, 10, 4319–4330, 958  
892 doi:10.5194/acp-10-4319-2010.

893 Wiegner, M., Emeis, S., Freudenthaler, V., Heese, B., Junkermann, W., Münkler, C., Schäfer, K.,  
894 Seefeldner, M., and Vogt, S.: Mixing layer height over Munich, Germany: variability and  
895 comparisons of different methodologies, *J. Geophys. Res.*, 111, D13201,  
896 doi:10.1029/2005JD006593, 2006.

897 Zhang, L., Jacob, D. J., Bowman, K. W., Logan, J. A., Turquety, S., Hudman, R. C., Li, Q., Beer,  
898 R., Worden, H. M., Worden, J. R., Rinsland, C. P., Kulawik, S. S., Lampel, M. C., Shephard, M.  
899 W., Fisher, B. M., Eldering, A., and Avery M. A.: Ozone-CO correlations determined by the  
900 TES satellite instrument in continental outflow regions, *Geophys. Res. Lett.*, 33, L18804,  
901 doi:10.1029/2006GL026399, 2006.

902

903

904

905

906 Tables

907 **Table 1.** Summary of information on the TRAQA and SAFMED flights.

908

Measurement campaign	Flight number	Date	Take off-landing time (UTC)	Departure-arrival	Geographic area investigated	<u>Description</u> <del>Events observed</del>
TRAQA 2012	V16	20/06/2012	13:12 – 16:34	Toulouse-Toulouse	Gulf of Lion	Test flight
	V17	22/06/2012	09:01 – 12:54	Toulouse-Toulouse	South-western France (over land) and the Atlantic Ocean	Test flight, biogenic emissions
	V18	26/06/2012	07:13 – 09:18	Toulouse-Bastia	Gulf of Genoa	Export of pollution from Northern Italy/Pô Valley, north- <del>we</del> easterly winds
	V19	26/06/2012	10:42 – 13:46	Bastia-Toulouse	Gulf of Genoa	Export of pollution from Northern Italy/Pô Valley, north- <del>we</del> easterly winds
	V20	27/06/2012	04:07 – 08:00	Toulouse-Nimes	Sea area south of Marseille/Toulon	Export of pollution during a Mistral-Tramontane event
	V21	27/06/2012	09:39 – 13:16	Nimes-Toulouse	Western coast of Corsica	Export of pollution from Northern Italy/Pô Valley, north- <del>we</del> easterly winds
	V22	29/06/2012	05:13 – 08:50	Toulouse-Bastia	Eastern coast of Corsica	Dust outbreak
	V23	29/06/2012	10:13 – 14:12	Bastia-Toulouse	Eastern and western coasts of Corsica	Dust outbreak
	V24	03/07/2012	13:19 – 17:12	Toulouse-Toulouse	Sea area north-east of Barcelona	Export of pollution from Barcelona, westerly/south-westerly winds
	V25	04/07/2012	07:18 – 10:54	Toulouse-Toulouse	Sea area south of Marseille/Toulon	Follow of Barcelona pollution plumes
	V26	04/07/2012	15:25 – 18:36	Toulouse-Toulouse	Gulf of Lion	Follow of Barcelona pollution plumes
	V27	06/07/2012	08:00 – 11.55	Toulouse-Toulouse	Sea area south of Marseille	Export of pollution during a moderate Mistral-Tramontane event
	V28	06/07/2012	14:01 – 17:45	Toulouse-Toulouse	Sea area south of Nice/Toulon	Export of pollution during a moderate Mistral-Tramontane event
	V29	07/07/2012	08:19 – 10:59	Toulouse-Nimes	Southern France (over land)	Biogenic emissions
	V30	07/07/2012	13:03 – 17:10	Nimes-Toulouse	Gulf of Genoa	Export of pollution during a moderate Mistral-Tramontane event
	V31	10/07/2012	13:41 – 17:21	Toulouse-Toulouse	Eastern coast of Spain	Characterization of pollution near coastal

						sources
	V32	11/07/2012	11:23 – 14:48	Toulouse-Toulouse	Southeastern coast of France and Gulf of Genoa	Characterization of pollution near coastal sources
SAFMED 2013	V46	24/07/2013	10:34 – 13:06	Genoa-Cagliari	Gulf of Genoa and eastern coast of Corsica and Sardinia	Characterization of pollution plumes in the Gulf of Genoa, Corsica, and Sardinia; westerly/south-westerly winds
	V47	24/07/2013	14:21 – 16:29	Cagliari-Genoa	Eastern coast of Corsica and Sardinia and Gulf of Genoa	Characterization of pollution plumes in the Gulf of Genoa, Corsica, and Sardinia; westerly/south-westerly winds
	V48	25/07/2013	13:12 – 16:02	Genoa-Ersa	Gulf of Genoa	Characterization of pollution in the Gulf of Genoa; westerly/south-westerly winds
	V49	27/07/2013	11:08 – 13:07	Genoa-Alghero	Central Italy (over land)	Characterization of pollution in central Italy
	V50	27/07/2013	15:33 – 16:48	Alghero-Genoa	Eastern coast of Corsica and Gulf of Genoa	Characterization of pollution plumes in the Gulf of Genoa, Corsica, and Sardinia; westerly/south-westerly winds + dust outbreak
	V51	30/07/2013	13:05 – 15:50	Genoa-Ersa	Gulf of Genoa	Characterization of pollution in the Gulf of Genoa; very low north/north-westerly winds
	V52	01/08/2013	12:03 – 15:24	Genoa-Alghero	Western coast of Corsica	Characterization of pollution in western Corsica; export of pollution from Northern Italy/Pô Valley; north-easterly winds

909  
910  
911  
912  
913  
914  
915  
916

917 **Table 2.** Comparison of the number concentrations  $dN_{\text{Aitken}}$  (0.004-0.1  $\mu\text{m}$ ) and  $dN_{\text{Acc}}$  (0.1-1.0  $\mu\text{m}$ )  
 918 observed during the TRAQA/SAFMED field campaigns with those reported in literature for  
 919 continental Europe. All literature data refer to airborne measurements.  
 920

<u>Atmospheric layer</u>	<u>Parameter</u>	<u>TRAQA/SAFMED</u>	<u>Literature over continental Europe</u>
<u>Free troposphere (FT)</u>	<u><math>dN_{\text{Aitken}}(\text{scm}^{-3})</math></u>	<u>0-19250</u>	<u>812-9149<sup>b</sup>; 0-980<sup>e</sup></u>
	<u><math>dN_{\text{Acc}}(\text{scm}^{-3})</math></u>	<u>34-3233</u>	<u>20-80<sup>a</sup>; 25-85<sup>c</sup>; 0-500<sup>f</sup></u>
<u>Boundary layer (BL)</u>	<u><math>dN_{\text{Aitken}}(\text{scm}^{-3})</math></u>	<u>4-22471</u>	<u>1037-31370<sup>b</sup>; 1000-20000<sup>c</sup>; 0-30000<sup>d</sup>; 0-19000<sup>e</sup></u>
	<u><math>dN_{\text{Acc}}(\text{scm}^{-3})</math></u>	<u>90-3215</u>	<u>70-560<sup>a</sup>; 10-50<sup>c</sup>; 400-1200<sup>e</sup>; 0-2000<sup>f</sup></u>

921  
 922 <sup>a</sup> Petzold et al. (2002), Central Europe, July-August 1998; size range  $dN_{\text{Acc}}(>0.15 \mu\text{m})$

923 <sup>b</sup> Mallet et al. (2005), Southeastern France, June 2001; size range  $dN_{\text{Aitken}}(0.006-0.6 \mu\text{m})$

924 <sup>c</sup> Wiegner et al. (2006), Germany, May 2003; ; size range  $dN_{\text{Aitken}}(>0.01 \mu\text{m})$ ,  $dN_{\text{Acc}}(>0.3 \mu\text{m})$

925 <sup>d</sup> Junkermann (2009), Po Valley, July-August 2002 and Septmeber-October 2003; ; size range  $dN_{\text{Aitken}}(>0.01 \mu\text{m})$

926 <sup>e</sup> Hamburger et al. (2012), central Europe, May 2008; size range  $dN_{\text{Aitken}}(0.004-0.15 \mu\text{m})$ ,  $dN_{\text{Acc}}(>0.15 \mu\text{m})$

927 <sup>f</sup> Highwood et al. (2012), central Europe, May 2008; size range  $dN_{\text{Aitken}}(0.004-0.15 \mu\text{m})$ ,  $dN_{\text{Acc}}(>0.15 \mu\text{m})$

928

929

930

931

932

933

934

935

936

937

938

939

940

941

942

943

944

945

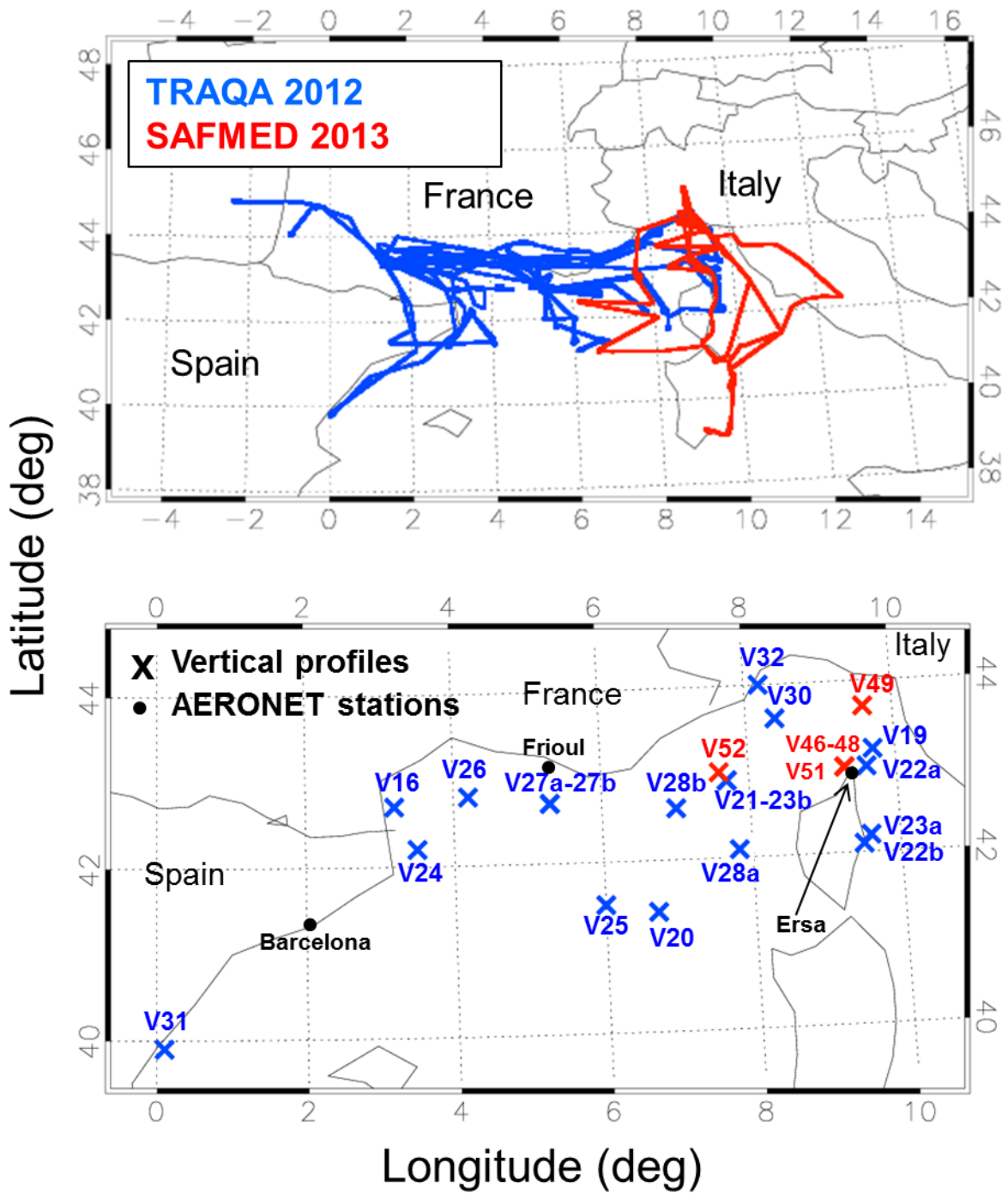
946

947

948

949 **Figures**

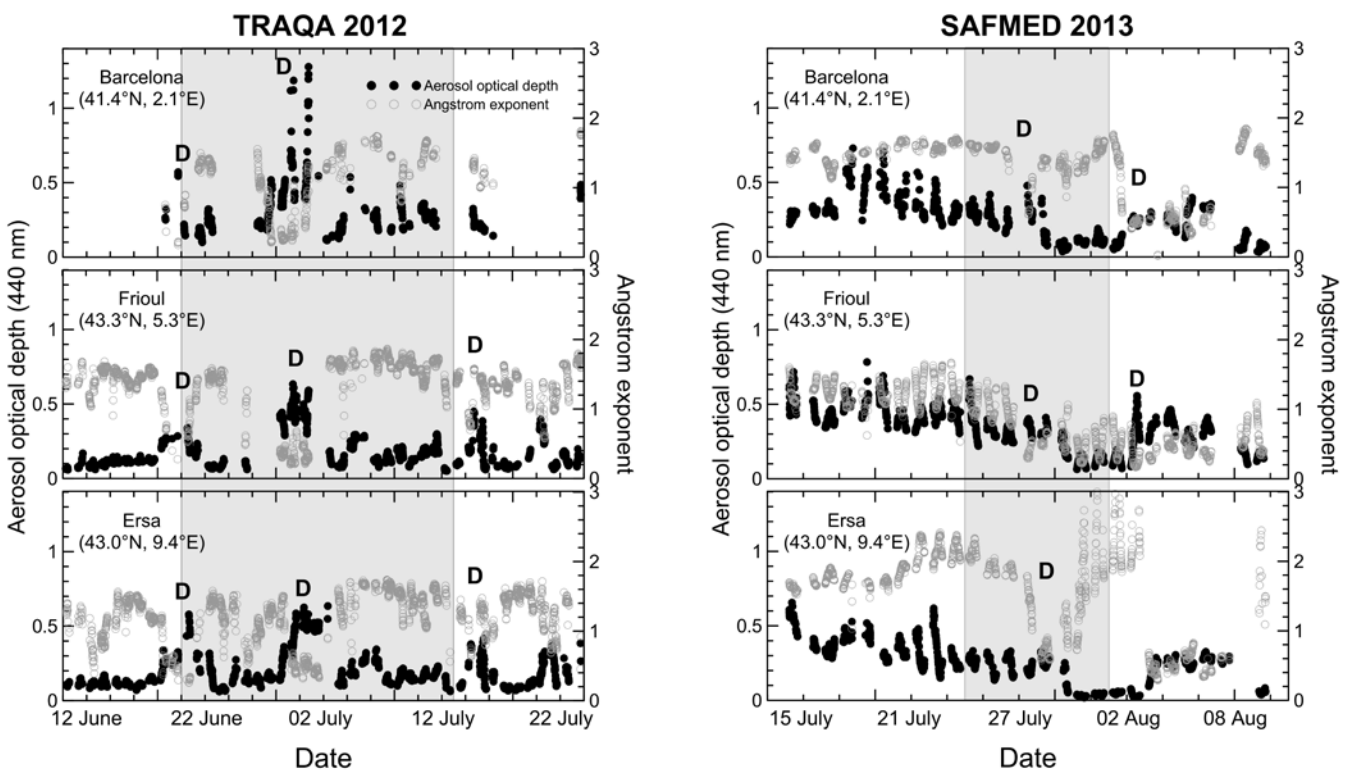
950 **Figure 1.** (Upper panel) Flight trajectories of the TRAQA (20 June - 13 July 2012) and the  
951 SAFMED (24 July - 1 August 2013) campaigns. The aircraft was based in Toulouse (43°36'N,  
952 1°26'E, France) during TRAQA and in Genoa (44°24'N, 8°55'E, Italy) during SAFMED. (Lower panel)  
953 Zoom on the investigated area and geographical position of the different vertical soundings  
954 analysed in this paper. The position of the three AERONET stations of Barcelona, Frioul, and Ersa  
955 considered in this study is also shown.  
956



958  
959  
960  
961

962  
963  
964  
965  
966  
967  
968  
969  
970  
971  
972  
973  
974  
975  
976

**Figure 2.** Aerosol optical depth at 440 nm ( $\tau$ ) and Ångström exponent ( $\alpha$ ) measured at the Barcelona, Frioul, and Ersa ~~different stations~~ AERONET stations in the Western Mediterranean basin during the TRAQA 2012 (left panels) and the SAFMED 2013 (right panels) campaigns. ~~Data are taken from the stations of Barcelona, Frioul, and Ersa located all around the basin.~~ The time period for the different plots is  $\pm 10$  days around the beginning/end of the two campaigns (data for the Barcelona station are not available over the entire period for 2012). The label D indicates the days affected by Saharan dust.

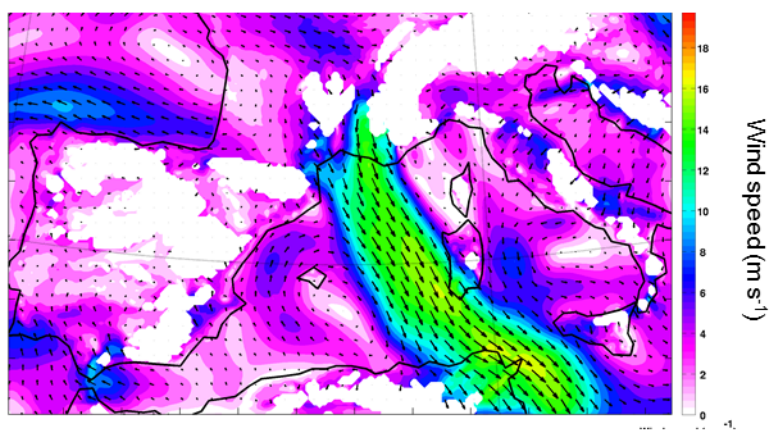


977  
978  
979  
980  
981  
982  
983  
984  
985  
986  
987

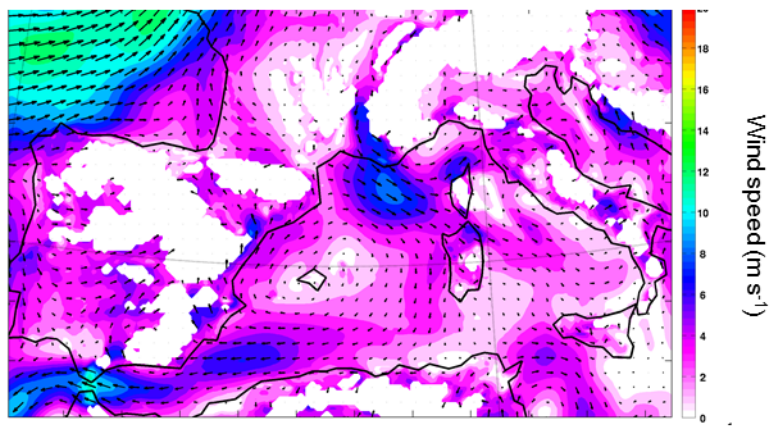
988  
989  
990  
991  
992  
993  
994  
995  
996

**Figure 3.** Example of wind maps at 925 mbar for 26 June and 3 July 2012. The maps are obtained from the WRF-Chem model (Weather Research and Forecasting – Chemistry) at 10-km horizontal resolution.

**a) 26 June 2012 12UT, 925 hPa**



**b) 03 July 2012 12UT, 925 hPa**



997  
998  
999  
1000  
1001  
1002  
1003

1004

1005

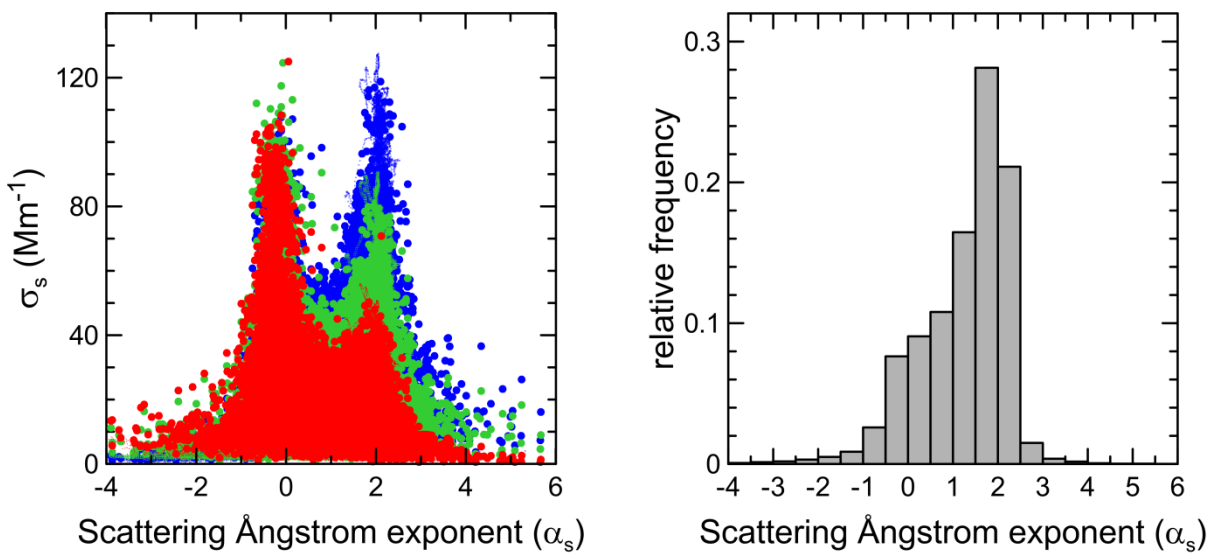
1006

1007

1008

1009 **Figure 4.** (Left) Scattering coefficient  $\sigma_s$  at 450, 550, and 700 nm versus the scattering Ångstrom  
1010 exponent  $\alpha_s$ . Cases with extremely negative ( $<-2$ ) and positive ( $>4$ ) values of  $\alpha_s$  are always related  
1011 with very low scattering coefficients, and are likely due to instrumental noise under low scattering  
1012 conditions. (Right) Frequency of occurrence of  $\alpha_s$  obtained considering vertical profiles data from  
1013 all TRAQA and SAFMED flights.

1014



1015

1016

1017

1018

1019

1020

1021

1022

1023

1024

1025

1026

1027

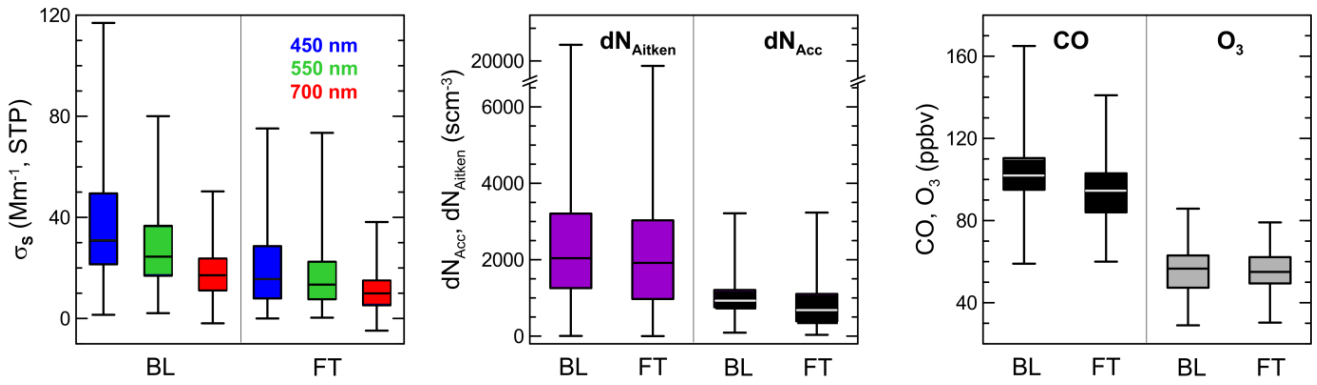
1028

1029



1030  
1031  
1032  
1033  
1034  
1035  
1036  
1037  
1038

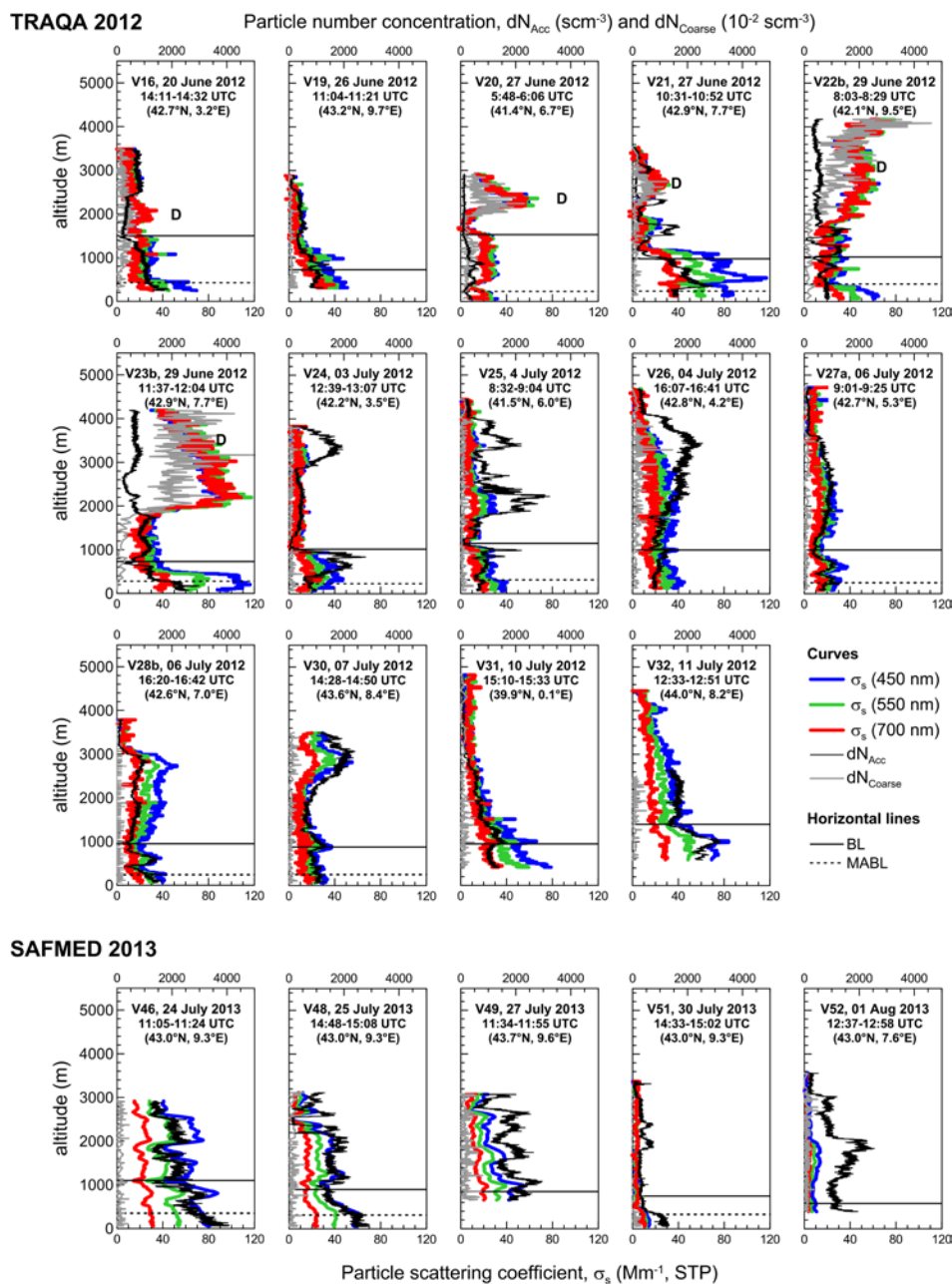
**Figure 5.** Box and whisker plot of the aerosol scattering coefficient ( $\sigma_s$ ) at 450, 550, and 700 nm, particle concentration in the Aitken ( $dN_{\text{Aitken}}$ ) and accumulation ( $dN_{\text{Acc}}$ ) modes, and CO and O<sub>3</sub> measured within pollution plumes in the boundary layer (BL) and in the free troposphere (FT).



1039  
1040  
1041  
1042  
1043  
1044  
1045  
1046  
1047  
1048  
1049  
1050  
1051  
1052  
1053  
1054  
1055  
1056  
1057  
1058  
1059  
1060  
1061  
1062  
1063  
1064  
1065  
1066  
1067  
1068

1069  
 1070  
 1071  
 1072  
 1073  
 1074  
 1075  
 1076  
 1077  
 1078  
 1079  
 1080  
 1081  
 1082  
 1083

**Figure 6.** Vertical profiles of the spectral scattering coefficient  $\sigma_s$  at 450, 550, and 700 nm and particle number concentration in the 0.1-1.0  $\mu\text{m}$  ( $dN_{\text{Acc}}$ ) and 1.0-4.0  $\mu\text{m}$  ( $dN_{\text{Coarse}}$ ) diameter ranges observed during TRAQA and SAFMED. Data are reported at STP (standard temperature and pressure,  $T = 293.15 \text{ K}$  and  $P = 1013.25 \text{ hPa}$ ). The heights of the top of the marine aerosol boundary layer (MABL) and planetary boundary layer (BL) estimated from the meteorological profiles are also indicated in the plots. The label D is used to identify the aerosol layers affected by Saharan dust. For certain flights (V22, V23, V27, and V28) two vertical soundings were performed; the letters “a” and “b” after the flight number in this plot specify if the considered data are taken from the first or the second sounding, respectively.



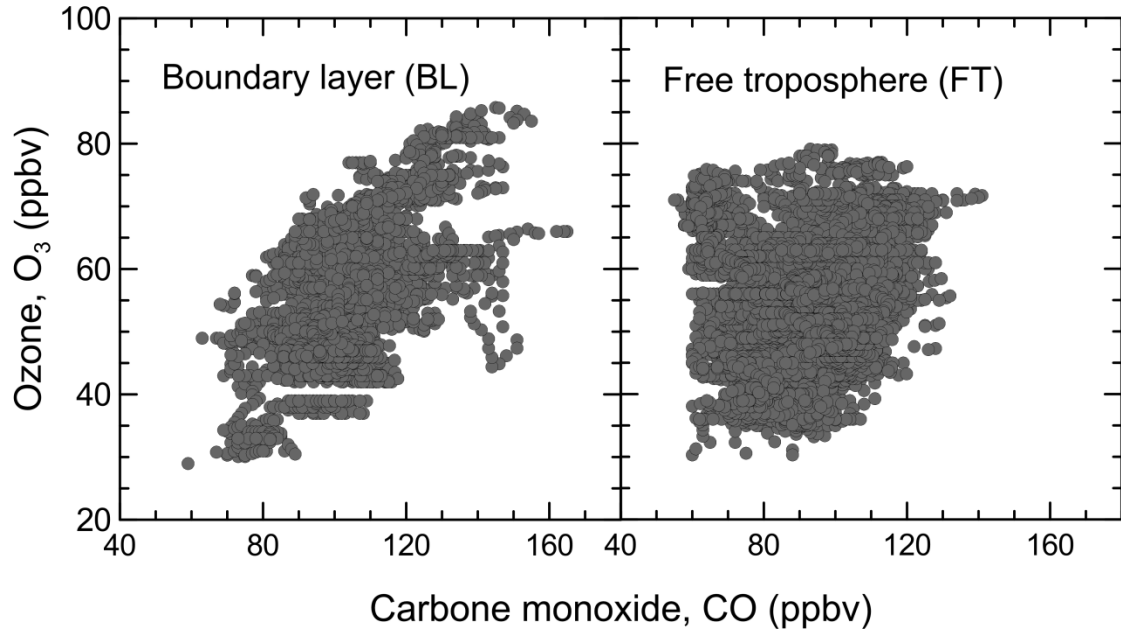
1084

1085

1086 **Figure 7.** O<sub>3</sub> versus CO in the boundary layer (BL) and the free troposphere (FT) for all TRAQA  
1087 and SAFMED vertical profiles (dust observations excluded).  
1088

1089

1090



1091

1092

1093

1094

1095

1096

1097

1098

1099

1100

1101

1102

1103

1104

1105

1106

1107

1108

1109

1110

1111

1112

1113

1114

1115

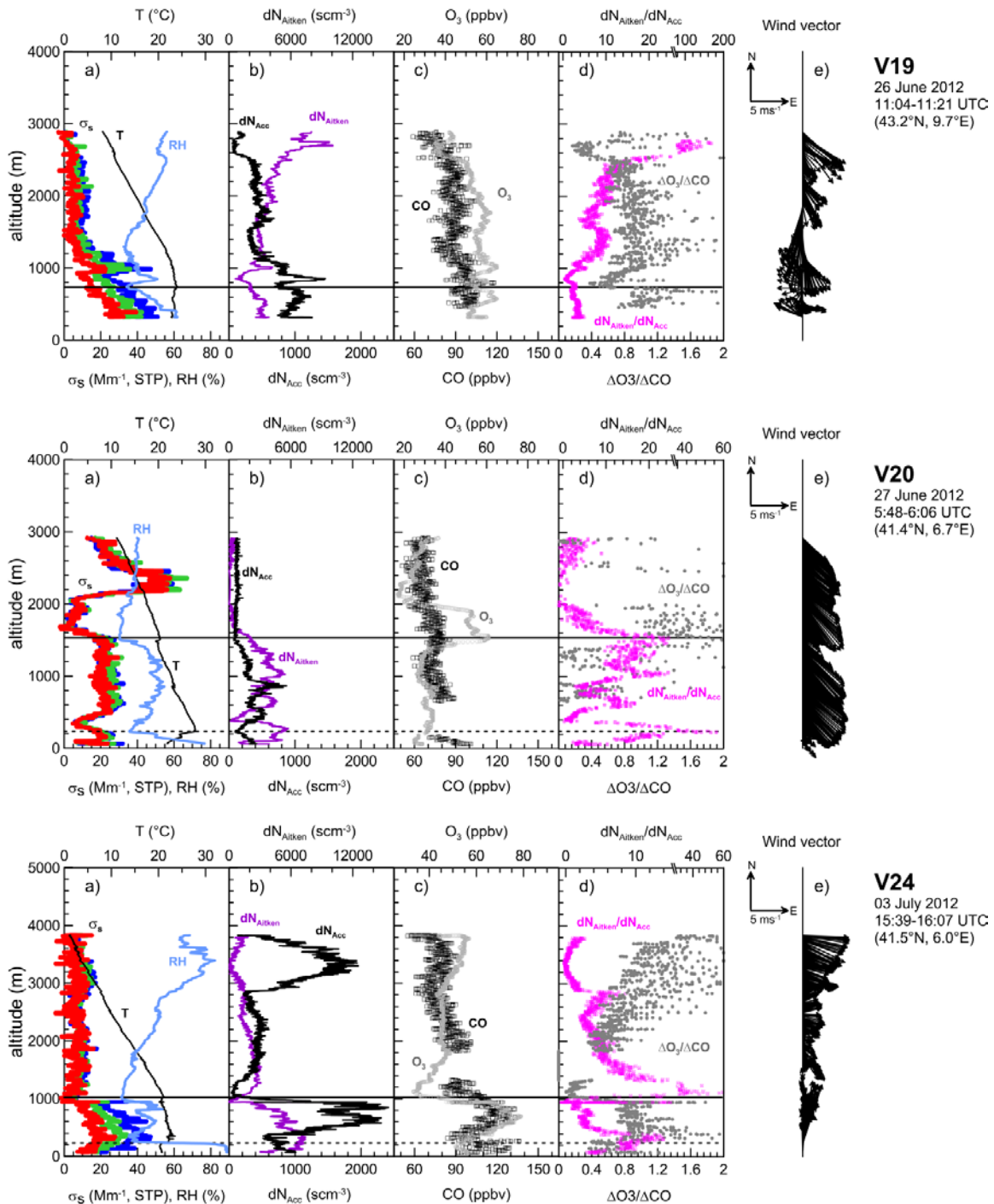
1116

1117

1118

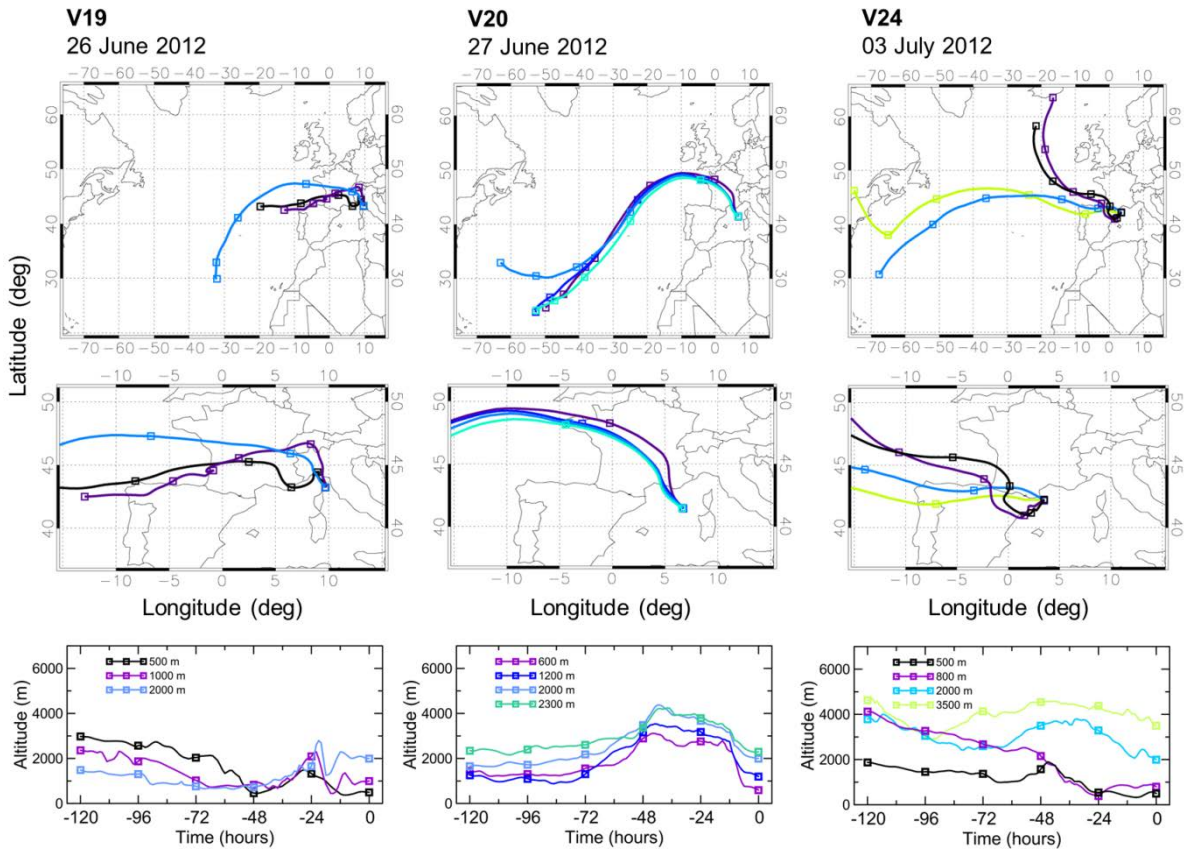
1119  
 1120  
 1121  
 1122  
 1123  
 1124  
 1125  
 1126  
 1127  
 1128  
 1129

**Figure 8.** Aerosol and trace gases vertical profiles for flights V19 (export from northern Italy/Po Valley), V20 (Mistral event), and V24 (export from the Barcelona area). The plots show the: (a) spectral scattering coefficient  $\sigma_s$  at 450, 550, and 700 nm (blue, green, and red lines, respectively), temperature (T, black line), and relative humidity (RH, light blue line); (b) particle number concentration in the 0.004-0.1  $\mu\text{m}$  ( $dN_{\text{Aitken}}$ , purple line) and 0.1-1.0  $\mu\text{m}$  ( $dN_{\text{Acc}}$ , black line) diameter ranges, (c) CO (black dots) and O<sub>3</sub> (grey dots) mixing ratios, (d) ozone enhancement factor  $\Delta\text{O}_3/\Delta\text{CO}$  (grey dots) and Aitken to accumulation ratio  $dN_{\text{Aitken}}/dN_{\text{Acc}}$  (pink dots) and (e) horizontal wind vector. The heights of the top of the MABL (dotted line) and BL (solid line) are also indicated.



1130

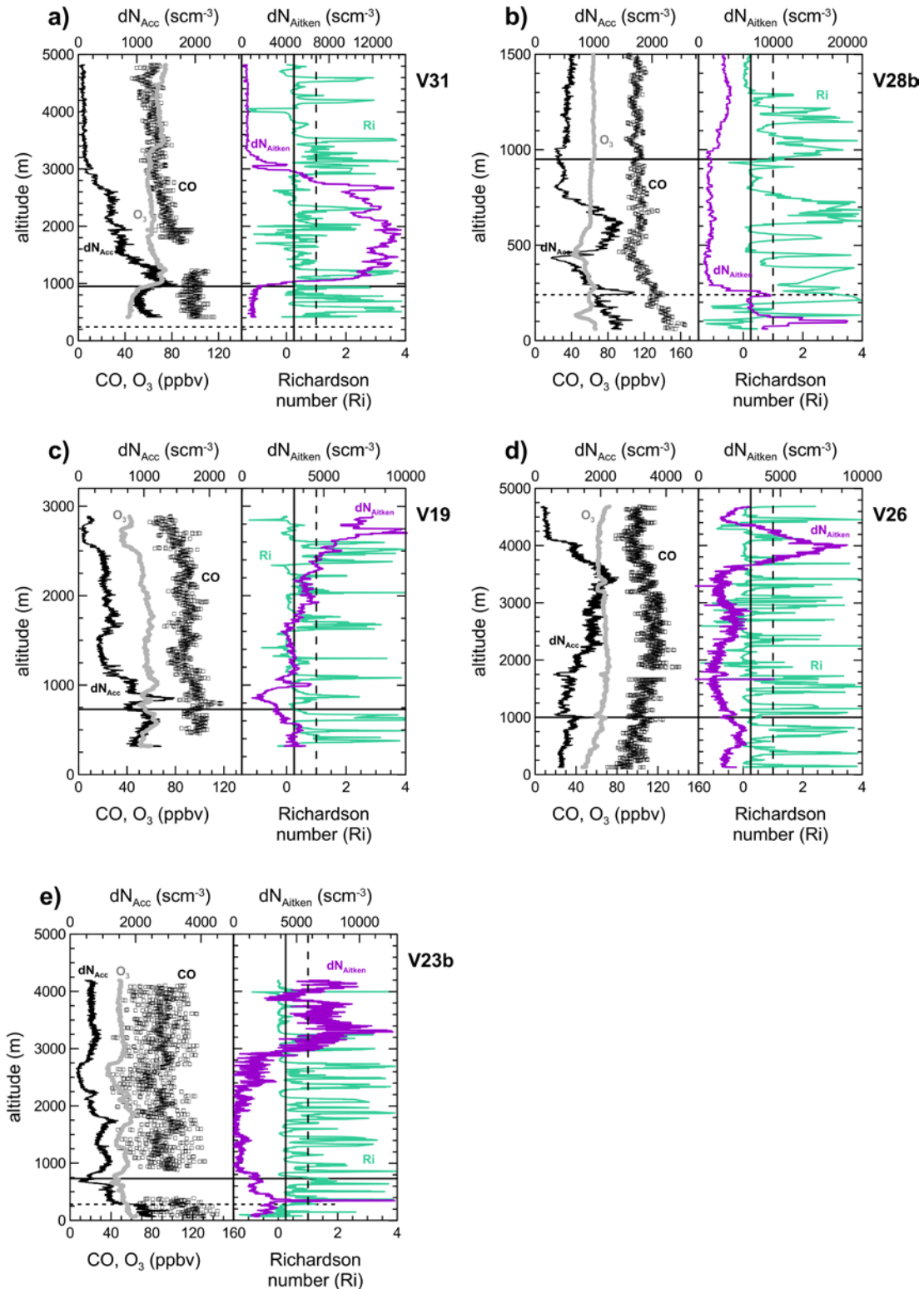
1131 **Figure 9.** Five-days backward air mass trajectories for the V19, V20, and V24 flights calculated  
 1132 with the FLEXTRA model. The upper panel shows the trajectories over an extended latitude-  
 1133 longitude region, while the central panel zooms on the Western Mediterranean area. The altitude of the  
 1134 air masses and its temporal evolution along the five days trajectories is reported in the lower  
 1135 panel of each plot.  
 1136



1137  
 1138  
 1139  
 1140  
 1141  
 1142  
 1143  
 1144  
 1145  
 1146  
 1147  
 1148  
 1149  
 1150

1151  
 1152  
 1153  
 1154  
 1155  
 1156  
 1157

**Figure 10.** Vertical profiles of the accumulation and Aitken particle concentrations ( $dN_{Acc}$ , black line, and  $dN_{Aitken}$ , purple line), CO (black dots), O<sub>3</sub> (grey dots), and gradient Richardson number (Ri, green line) for flights a) V31, b) V28, c) V19, d) V26 and e) V23b. The horizontal lines indicate the height of the marine boundary layer MABL (dotted line) and the planetary boundary layer BL (continuous line), while the vertical lines indicate  $Ri_{crit}=0.25$  and  $Ri=1$  (continuous and dashed lines, respectively).



1158